ACCSCIENCE PUBLISHING

International Journal of Bioprinting

ACCEPTED PAPER · MAIN TEXT

Development and biological validation of a dexamethasone-loaded, PLA-based 3D-printable composite filament for bone tissue engineering

Article ID: IJB026200186

Citation: Bianconi S, Asci C, Ott F, *et al*. Development and biological validation of a dexamethasone-loaded, PLA-based 3D-printable composite filament for bone tissue engineering. *Int J Bioprint*. 2026. doi: 10.36922/IJB026200186

AccScience Publishing
RESEARCH ARTICLE
Volume X Issue X (2026)
doi: 10.36922/IJB026200186

Development and biological validation of a dexamethasone-loaded, PLA-based 3D-printable composite filament for bone tissue engineering

Running title: Dexamethasone–PLA filament for bone repair

Santiago Bianconi[1]*, Cem Asci[1], Fiona Ott[1], Ferdinand Mehnert[1], Robert Heidrich[2,3], Michael Wendt[2], Minhong Wang[1], Lea Usov[1], Ingo Marzi[1], Dirk Henrich[1], and Jonas Neijhoft[1]

[1] Department of Trauma Surgery and Orthopedics, University Hospital, Goethe University Frankfurt, Theodor-Stern-Kai 7, Frankfurt am Main, D-60590, Germany
[2] Fraunhofer CSP, Otto-Eißfeldt-Strasse 12, Halle (Saale), 06120, Germany
[3] Anhalt University of Applied Sciences, Bernburger Strasse 55, Koethen, 06366, Germany

*** Corresponding author:**
Santiago Bianconi (bianconi@med.uni-frankfurt.de)

Citation: Bianconi S, Asci C, Ott F, *et al*. Development and biological validation of a dexamethasone-loaded, PLA-based 3D-printable composite filament for bone tissue engineering. *Int J Bioprint.* 2026. doi: 10.36922/IJB026200186

Received: May 12, 2026
Revised: July 1, 2026
Accepted: July 8, 2026
Published online: July 8, 2026

Abstract

Critical-sized bone defects remain a major therapeutic challenge. Among additive manufacturing approaches, fused filament fabrication provides a scalable alternative to autografting by enabling the production of patient-specific scaffolds with integrated bioactive functionality. Given the osteogenic and immunomodulatory properties of dexamethasone (DEXA), this study aimed to develop a 3D-printable DEXA-loaded polylactic acid (PLA) composite filament for controlled local drug delivery and to assess its osteogenic and immunomodulatory effects in vitro. DEXA–PLA composite filaments (0.1% and 1% w/w) were fabricated by melt extrusion. Thermal, chemical, surface, and mechanical characterization were performed using thermogravimetric analysis, differential scanning calorimetry, dynamic mechanical analysis, Fourier-transform infrared spectroscopy, contact angle, and three-point bending tests. DEXA release over 28 days was quantified by ELISA. Human mesenchymal stromal cells (MSCs) or THP-1–derived macrophages (TDM) were cultured in indirect contact with PLA or DEXA–PLA (0.1% or 1%) test specimens or treated with soluble DEXA as positive control. Osteogenic and immunomodulatory effects were assessed by metabolic activity (resazurin assay), gene expression (RT-qPCR), extracellular matrix (ECM) mineralization (Alizarin Red quantification), and cytokine secretion (Cytometric Bead Array). Statistical analysis was performed using two-way ANOVA followed by Tukey's multiple comparisons test, and Kruskal–Wallis/Dunn ($n = 4$; $\alpha = 0.05$). Thermal, chemical, surface, and mechanical properties of CF are largely preserved after DEXA incorporation. Both formulations exhibited distinct, concentration-dependent release kinetics. While the 0.1% DEXA–PLA showed a transient increase in DEXA concentration up to 72 h followed by decline, the 1% DEXA–PLA established a sustained plateau (~143 ng of DEXA per g of test specimen) over 28 days. Neither composite affected MSC metabolic activity. After 14 days, the 1% DEXA–PLA significantly enhanced *ALPL* expression and ECM mineralization compared with the 0.1% DEXA–PLA and PLA, reaching levels comparable to osteogenic differentiation medium (10 nM DEXA). In macrophages, the 1% DEXA–PLA selectively reduced in M1 cells metabolic activity, *IL1B* expression and secretion of IL-1β, IL-6, and TNF-α, while upregulating *CD163* and *PPARG*. The FFF-compatible 1% DEXA–PLA CF retains physicochemical integrity after DEXA incorporation and enables sustained local DEXA delivery within a biologically active concentration range, achieving dual osteogenic and immunomodulatory effects, as evidenced by attenuated M1 macrophage activation. These findings demonstrate the feasibility of integrating DEXA into a controlled drug release system for bone tissue engineering applications.

Keywords: Additive manufacturing; 3D printing; Dexamethasone; Bone tissue engineering

1. Introduction

Critical-sized bone defects remain a major clinical challenge, and current gold-standard treatments such as autologous bone grafting are limited by material availability and donor-site morbidity (reviewed in [1,2]). Bone tissue engineering (BTE) has emerged as a promising strategy to overcome these limitations, through engineered scaffolds (reviewed in [3]). However, clinical translation remains limited, particularly due to challenges related to scalability, cost-effectiveness, standardization and patient-specific adaptability [4].

Additive manufacturing, particularly fused filament fabrication (FFF), has emerged as a powerful approach to produce patient-specific scaffolds with controlled architecture and mechanical properties in a reproducible and cost-efficient manner (reviewed in [5,6]). Beyond structural design, current developments increasingly focus on imparting biological functionality to additively manufactured scaffolds to actively regulate the cellular environment at the defect site [7]. In this context, the incorporation of bioactive molecules directly into printable polymer matrices enables localized and sustained delivery without additional complex post-processing steps [8].

Among thermoplastic polymers suitable for FFF, polylactic acid (PLA) is widely used due to its biocompatibility, biodegradability, low toxicity, and established processability [9,10]. Importantly, PLA can also serve as a carrier for bioactive compounds, enabling the fabrication of drug-loaded composite filaments for additive manufacturing applications (reviewed in [11]).

Dexamethasone (DEXA) is a synthetic glucocorticoid (GC) known to promote osteogenic differentiation of mesenchymal stromal cells (MSCs) and modulate inflammatory responses during tissue repair [12,13]. However, prolonged or systemic exposure to high DEXA concentrations is associated with adverse side effects, emphasizing the need for localized and controlled delivery strategies [14-17].

Several studies have reported the incorporation of bioactive agents into thermoplastic polymers suitable for additive manufacturing in the context of BTE, including inorganic materials such as bioglass, biological factors such as bone morphogenetic proteins, and pharmaceuticals including statins or antibiotics (e.g., vancomycin and rifampicin) [18-24]. DEXA has likewise been incorporated into composite filaments and additively manufactured constructs using various material systems and fabrication strategies [8,25-27]. However, studies investigating DEXA-loaded PLA composite filaments produced directly by melt extrusion remain limited.

We hypothesized that DEXA could be successfully incorporated into a PLA matrix by melt extrusion and subsequently processed by FFF without substantial loss of bioactivity, resulting in constructs that retain osteogenic and immunomodulatory properties.

In this study, we developed a PLA-based, DEXA-loaded composite filament compatible with FFF to enable controlled local drug release from printed constructs. We systematically investigated the physicochemical properties and release kinetics of two DEXA loadings (0.1% and 1%) and evaluated their biological effects on the OD of human MSCs and the polarization of macrophages derived from the immortalized THP-1 cell line. By integrating a scalable fabrication strategy with dual osteogenic and immunomodulatory functionality, this work aims to advance the development of bioinstructive additively manufactured constructs for BTE applications.

2. Materials and methods

2.1. Fabrication of DEXA-loaded PLA composite filaments

DEXA-loaded PLA (DEXA–PLA) composite filaments (1.75 mm target diameter) were fabricated by melt extrusion using PLA Ingeo Biopolymer PLA 4043D (Natureworks, Plymouth, MN, USA) as the polymer matrix (Figure 1A). PLA granules (nominal size 1–3 mm, molecular weight 110,000–143,700 g/mol) [28,29] were ground to a particle size of 0.25–1 mm using a shredder (QITech Industries GmbH, Darmstadt, Germany) and subsequently dried at 40°C for 24 h to reduce residual moisture prior to processing.

To promote homogeneous drug distribution and prevent segregation during feeding and extrusion, a silicone-assisted pre-coating step was applied as previously described [30]. Briefly, shredded PLA granules were transferred into a 50 mL conical tube and coated with three drops of silicone oil (~60–90 mg per 10 g PLA; J. Harhaus, Radevormwald, Germany). The granules were vortexed for 1 min and then transferred into a fresh tube to avoid wall-retained residues and ensure clean blending conditions.

Under continuous vortexing, dexamethasone phosphate disodium salt powder (AdipoGen, Füllinsdorf, Switzerland) was incrementally added to the pre-coated PLA until the target concentrations of 0.1% or 1% (w/w) were reached. Drug-free PLA control filaments underwent the identical silicone pre-coating and vortexing procedure to ensure comparable processing conditions. Dexamethasone phosphate disodium salt is a highly water-soluble glucocorticoid prodrug that exhibit a melting point between 233–240 °C with decomposition onset ≥233 °C. This thermal behavior is compatible with our melt-extrusion processing conditions for PLA (176–189 °C), providing a 44–64 °C safety margin below decomposition and supporting its incorporation into thermoplastic filaments for fused filament fabrication [31].

The resulting PLA and DEXA–PLA mixtures were melt-extruded (Figure 1B) using a modified single-screw filament extruder (Maker one composer, 3devo, Utrecht, The Netherlands) at a

screw speed of 5.6 rpm with starve-fed granulate addition. The extrusion temperature profile was set to 176–184–189–175°C, and the cooling fan was operated at 65%. These parameters were selected to provide sufficient shear for homogeneous composite formation while avoiding excessive melt pressure.

To ensure continuous material flow during extrusion and to reliably process the low batch size (10 g), 100 mg of black filament was added at the end of each batch. The appearance of this marker material at the extruder nozzle indicated completion of the filament and ensured consistent filler dosing. Filament diameter was monitored throughout the process, targeting 1.75 ± 0.5 mm. All formulations (PLA, 0.1% DEXA–PLA, and 1% DEXA–PLA) yielded dimensionally stable filaments suitable for FFF (Figure 1C).

2.2. Digital microscopic analysis of filament appearance and surface integrity

Images of PLA and DEXA–PLA composite filaments were acquired using a Keyence digital microscope (VHX-X1) equipped with a standard objective (VH-Z20) at 100× magnification with brightfield (epi-illumination) and darkfield (ring illumination) (Keyence, Osaka, Japan).

2.3. Thermal and thermomechanical characterization of DEXA-loaded PLA composites

2.3.1. Sample preparation

For thermogravimetric analysis (TGA) and differential scanning calorimetry (DSC), filament specimens with masses between 15 and 18 mg were analyzed. For dynamic mechanical analysis (DMA), the filament samples were cut to a length of 15 mm. The filament diameter was determined to be 1.7 mm using a micrometer (Mitutoyo 293-821, Tokyo, Japan) with a resolution of 0.001 mm. Depending on the analysis, samples were placed in either open Al_2O_3 crucibles (TGA) or 25 µL aluminum crucibles with pierced lids (DSC). Sample masses were determined using either the instrument's internal balance (TGA) or a Mettler Toledo XS205DU balance (Uster, Switzerland). Each measurement was performed in duplicate, and all raw data were processed using OriginPro 2025b (OriginLab Corporation, Northampton, MA, USA).

2.3.2. Thermogravimetric analysis

To determine the thermal stability of the filament samples, a NETZSCH TGA 209 F1 Iris (Selb, Germany) was used. Measurements were conducted under N2 atmosphere (20 mL/min) by heating the samples from 25 °C to 900 °C at 10 K/min. The onset temperatures (T_{onset}) were determined using the tangent method according to DIN EN ISO 11358-1:2022-07 [32].

2.3.3. Differential scanning calorimetry

The non-isothermal experiments were carried out using a NETZSCH DSC 204 F1 Phoenix, (Selb, Germany). The heat flow versus temperature curves were measured in a temperature range of -20 °C to 220 °C under N2 atmosphere (20 mL/min) at a heating rate of 10 K/min. Two heating runs were carried out. After the first heating cycle, the samples were cooled to −20 °C at 10 K/min and subsequently reheated under identical conditions. The glass transition temperature (T_g), the enthalpies of crystallization (H_c) and melting (H_m), and the melting temperature (T_m) were determined in accordance with DIN EN ISO 11357 [33].

2.3.4. Dynamic mechanical analysis

The measurements were performed from 25 °C to 90 °C at a constant heating rate of 3 K/min with a NETZSCH DMA 242C (Selb, Germany). The DMA measurement length was 10 mm. The determination of the storage modulus E' and the loss factor tan(δ) was performed in tensile mode at a measurement frequency of 1 Hz and an amplitude of 30 µm. The T_g and the T_{onset} were calculated in accordance with DIN EN ISO 6721-1:2019-09 [34].

2.4. Structural and chemical characterization of DEXA-loaded PLA composites

2.4.1. Fourier-transform infrared spectroscopy

The chemical structure of PLA and DEXA-loaded PLA filaments was analyzed using Fourier-transform infrared spectroscopy (FTIR) in attenuated total reflection (ATR) mode. FTIR spectra were acquired using a Thermo Scientific Nicolet iS20 spectrometer equipped with a diamond ATR crystal and a DTGS KBr detector (Karlsruhe, Germany). A background spectrum was recorded prior to the measurements and automatically subtracted from the sample spectra. An atmospheric correction was also performed. Each sample was measured in triplicate with 16 scans each. The gain factor was set to 1 (no signal amplification). A data resolution of 0.48 cm^{-1} was achieved through zero-filling. Spectra were processed in Python using baseline correction with the asls algorithm (pybaselines), followed by normalization to the integrated CH_3 band (1480–1430 cm^{-1}) and graphical visualization [35-37]. Graphs were generated using the matplotlib library [38].

2.4.2. Thermal aging of DEXA-loaded PLA composites

Aging experiments were conducted on PLA and DEXA-loaded PLA filaments using a Thermo Scientific Heratherm convection oven (Cleveland, OH, USA) at 150 °C for 48 h prior to FTIR analysis to assess their thermal aging stability and potential susceptibility to thermo-oxidative changes under ambient air conditions.

2.5. Surface wettability assessment of test specimens made of DEXA-loaded PLA composites

The surface wettability of 3D-printed disc-shaped test specimens (TS, 5 mm diameter × 0.8 mm height) made of PLA or DEXA-loaded PLA filaments was evaluated by static water contact angle measurements using the principle of the sessile drop method. Measurements were performed with a Keyence digital microscope (VHX-X1) equipped with a standard objective (VH-Z20) and a free-angle observation system (VHX-S750E) enabling side-view imaging (Keyence, Osaka, Japan). Distilled water droplets (8 µL) were deposited onto the specimen surface using a micropipette. Images were acquired 10 s after droplet deposition under ambient conditions (23 ± 2 °C, 50 ± 10% relative humidity). Contact angles were determined using the manual angle measurement tool of the VHX-X1 software (v3.2.22.472). The angle between the specimen surface baseline and the tangent to the droplet profile at the three-phase contact point was measured on both sides of the droplet and averaged. Ten measurements were performed at different, previously unused locations on each specimen to account for surface heterogeneity associated with the layer-by-layer manufacturing process.

2.6. Mechanical performance of test specimens made of DEXA-loaded PLA composites

The flexural properties of 3D-printed rectangular specimens (50 mm × 6 mm × 1 mm height) made of PLA or DEXA-loaded PLA filaments, in accordance with DIN EN ISO 178, were determined using a destructive three-point bending test on a table-top testing machine (Zwick/Roell ZwickiLine 5.0, Zwick-Roell, Ulm, Germany) [39]. Specimens were conditioned at room temperature and then placed on two bars, spaced 16 mm apart and tested by loading at the midpoint using a plunger speed of 2 mm/min until failure. Load and displacement were recorded continuously, and flexural modulus and maximum load were calculated from the resulting load–displacement curves using TestXpert II software (version 3.3, Zwick-Roell, Ulm, Germany) [30].

2.7. 3D printing of test specimens for in vitro studies

Disc-shaped TS (5 mm diameter × 0.8 mm height; surface area ≈ 52 mm²; mass ≈ 25 mg; layer height 0.2 mm; total layers 4; Figure 1D) were produced by FFF using a modified cartesian direct-drive extruder 3d-printer (Ender-2, Creality, Shenzhen, China) inside a S2020 Class II safety cabinet (Thermo Scientific, Langenseldbold, Germany) to maintain sterility (Figure 1E). Printing parameters included a 0.4 mm nozzle diameter, 10 mm/s speed, 185°C nozzle temperature, and 25°C build plate temperature [24].

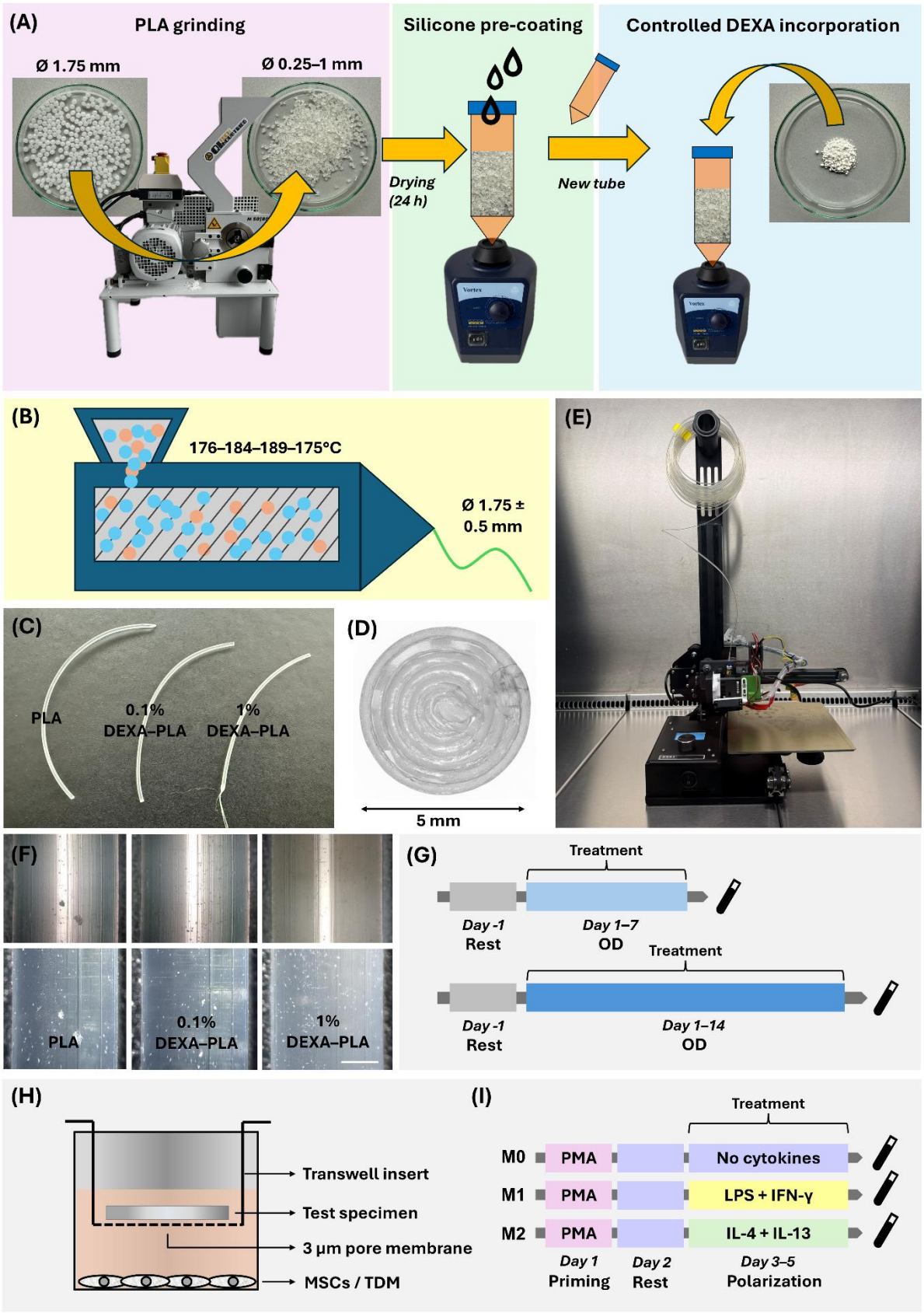

Figure 1. Fabrication of DEXA-loaded PLA (DEXA–PLA) composite filaments, 3D printing of test specimens (TS), and experimental design. (A) DEXA–PLA feedstock preparation. (B) Filament fabrication by melt extrusion. (C) Extruded PLA and DEXA–PLA composite

filaments. (D) Representative disc-shaped TS (5 mm diameter × 0.8 mm height; surface area ≈ 52 mm²; mass ≈ 25 mg; layer height 0.2 mm; total layers 4) utilized for in vitro assays. (E) Sterile TS fabrication using FFF. (F) Representative digital microscopic images showing the surface morphology and transparency of PLA and DEXA–PLA composite filaments under brightfield (top) and darkfield (bottom) illumination. Scale bar = 500 µm. (G) Experimental timeline for osteogenic differentiation (OD) of mesenchymal stromal cells (MSCs). (H) Schematic representation of the cell culture system for treatment with PLA or DEXA–PLA composite filaments. (I) Experimental timeline for priming and polarization of THP-1–derived macrophages (TDM). Phorbol 12-myristate 13-acetate (PMA), lipopolysaccharide (LPS), interferon-gamma (IFN-γ), interleukin 4 (IL-4), interleukin 13 (IL-13).

2.8. DEXA release from DEXA-loaded PLA composite filaments

2.8.1. DEXA concentration profile over time

DEXA appearance profile was assessed using disc-shaped TS fabricated from PLA, 0.1% DEXA–PLA, and 1% DEXA–PLA composite filaments, as described above. Individual specimens were placed into single wells of a 96-well plate and incubated at 37°C with 100 µL of Ca^{2+}/Mg^{2+}-free PBS (Gibco, Paisley, UK) which allows drug diffusion avoiding the presence of proteins. Concentration was evaluated at 1 h, 3 h, 6 h, 24 h, 72 h, 7 d, and 28 d, using separate specimens for each sampling interval. At each time point, PBS was collected from individual wells and stored at −80°C until analysis.

2.8.2. DEXA quantification by ELISA

DEXA concentrations in the collected samples were quantified using a competitive ELISA specific for DEXA (Cusabio, Houston, TX, USA) according to the manufacturer's instructions. Absorbance was measured at 450 nm using a microplate reader.

2.9. Effect of DEXA-loaded PLA composite filaments on osteogenic differentiation of MSCs

2.9.1. Cell culture of pooled MSCs

A human MSC pool was generated from residual bone marrow samples from five healthy donors. Ethical approval for the use of these samples for research purposes was granted by the Ethics Committee of the Department of Medicine, Goethe University Frankfurt (approval number 329/10). All donors provided written informed consent prior to sample collection. MSCs were isolated by plastic adherence, expanded for 14 days in T175 cell culture flasks (Sarstedt, Nümbrecht, Germany), and cryopreserved in small aliquots (1×10^6 cells in 1 mL of

cryopreservation medium consisting of 25% human serum from human male AB plasma and 10% DMSO (Sigma-Aldrich, St. Louis, MO, USA) in GlutaMAX™ DMEM low glucose (Gibco, Thermo Fisher Scientific, Dreieich, Germany)). The isolated MSCs exhibited a typical MSC phenotype ($CD73^+$, $CD90^+$, $CD105^+$, $CD45^-$, $CD34^-$) and demonstrated trilineage differentiation potential [24].

For subculture, 3.5×10^5 MSCs were seeded into T175 cell culture flasks (Sarstedt, Nümbrecht, Germany) and maintained in 25 mL of animal component-free growth medium (GM) consisting of 5% heparin-free PLTGold® human platelet lysate (Merck KGaA, Darmstadt, Germany) in GlutaMAX™ DMEM low glucose (Gibco, Thermo Fisher Scientific, Dreieich, Germany). Cultures were maintained at 37°C in a humidified atmosphere containing 5% CO_2 and 21% O_2. The culture medium was replaced every 3–4 days, and cells were expanded until 80% confluence, detached with 3.5 mL of 0.05 % Trypsin-EDTA (Gibco, Thermo Fisher Scientific, Dreieich, Germany), and passaged until use in subsequent experiments.

2.9.2. Osteogenic differentiation treatment of MSCs

Cells at passage 6 were seeded into 24-well plates at a density of 1×10^4 cells per well and cultured for 24 h in 1 mL of GM to allow cell adhesion. Cells were then assigned to one of the seven experimental conditions (Table 1) and treated for one or two weeks (Figure 1G). DEXA-free OD medium consisted of GM supplemented with 10 mM β-glycerophosphate disodium salt hydrate and 50 µM ascorbic acid 2-phosphate (Sigma-Aldrich, St. Louis, MO, USA), and DEXA-containing OD medium (positive controls) consisted of OD medium supplemented with 10 nM or 100 nM DEXA (Sigma-Aldrich, St. Louis, MO, USA) to probe dose-dependent osteogenic responses across a commonly used in vitro concentration range (reviewed in [40]). To evaluate the effects of DEXA–PLA composite filaments, cells were cultured in 1 mL of DF-ODM and TS were placed in contact with the culture medium using 6.5-mm Transwell® membrane inserts for 24-well plates (3 µm pore size, polycarbonate; Corning, Wiesbaden, Germany) (Figure 1H). After 7 or 14 days of culture, metabolic activity (MA) was assessed using the resazurin reduction assay while OD was assessed by Alizarin Red S staining and quantification, as well as by gene expression analysis of osteogenic markers.

Table 1. Experimental groups used to assess the effects of DEXA–PLA composite filaments on osteogenic differentiation of MSCs

Group	Composite filament	DF-ODM	Soluble DEXA
Negative control	–	–	–
DF-ODM	–	+	–

ODM (10 nM DEXA)	–	+	+
ODM (100 nM DEXA)	–	+	+
DF-ODM + PLA	PLA	+	–
DF-ODM + 0.1% DEXA–PLA	0.1% DEXA–PLA	+	–
DF-ODM + 1% DEXA–PLA	1% DEXA–PLA	+	–

DEXA, dexamethasone; PLA, polylactic acid; DF, DEXA-free; ODM, osteogenic differentiation medium.

2.9.3. Alizarin red S staining

To evaluate extracellular matrix mineralization by MSCs, cell layers were fixed with 0.5 mL per well of 4% (v/v) formaldehyde (Roti-Histofix 4%, Carl Roth, Karlsruhe, Germany), rinsed twice with 1 mL per well of distilled water and stained with 0.5 mL per well of alizarin red (AR) S monosodium salt (40 mM, pH 4.1–4.3; Sigma-Aldrich, Merck KGaA, Darmstadt, Germany) for 20 min. Excess dye was removed by thorough washing with distilled water. After removal of residual water, stained cell monolayers were visualized by phase-contrast microscopy using an inverted microscope (BZ-X810, Keyence, Osaka, Japan) and stored at −20°C until further processing.

2.9.4. Spectrophotometric quantification of alizarin red S staining

Frozen plates were thawed at room temperature, and 200 µL of 10% (v/v) acetic acid (JT Baker, Deventer, Holland) was added to each well, followed by incubation for 20 min at room temperature with gentle agitation (100 rpm). The resulting cell lysate was collected using a pipette tip and completely transferred to microcentrifuge tubes. Samples were heated to 85°C for 10 min, subsequently cooled on ice for 5 min, and then centrifuged at 16,000 × g for 15 min. The supernatant was transferred to fresh microcentrifuge tubes and neutralized by the addition of 75 µL of 10% (v/v) ammonium hydroxide (Fluka Chemie, Steinheim, Germany), followed by brief vortexing. Subsequently, 50 µL of each sample was transferred in duplicate to a 96-well plate. A blank consisting of 200 µL of 10% acetic acid mixed with 75 µL of 10% ammonium hydroxide was included. Absorbance was measured at 405 nm using a spectrophotometer (Infinite 200 Pro, Tecan, Grödig, Austria).

2.10. Effect of DEXA-loaded PLA composite filaments on polarization of THP-1–derived macrophages

2.10.1. Cell culture of THP-1 cells

THP-1 human monocytic cells (TIB-202) were obtained from the European Collection of Authenticated Cell Cultures (ECACC) and used as received. The cells were cultured in T75 cell culture flasks (Sarstedt, Nümbrecht, Germany) positioned vertically and containing 21 mL of macrophage GM consisting of 10% fetal bovine serum (Gibco, Paisley, UK), 100 U/mL penicillin, and 100 µg/mL streptomycin (Sigma-Aldrich, St. Louis, MO, USA) in RPMI 1640 medium with L-glutamine (Gibco, Paisley, UK). Cultures were maintained at 37°C in a humidified atmosphere containing 5% CO_2. Approximately half of the medium volume was replaced with fresh GM every 3-4 days.

2.10.2. THP-1 cell priming and polarization

For differentiation into macrophage-like cells, 3.5×10^5 THP-1 cells suspended in 1 mL of macrophage GM were seeded per well in 24-well cell+ plates (Sarstedt, Nümbrecht, Germany) and incubated for 24 h in the presence of 5 ng/mL phorbol 12-myristate 13-acetate (PMA, Sigma-Aldrich, Taufkirchen, Germany). This PMA concentration has been reported to induce stable macrophage differentiation without excessive gene upregulation [41]. Following priming, the culture medium and non-adherent cells were completely removed, and adherent cells were washed twice with 1 mL of sterile Ca^{2+}/Mg^{2+}-free PBS. Fresh macrophage GM (1 mL per well) was then added, and cells were allowed to rest for 24 h. Subsequently, macrophage polarization was induced for 72 h (Figure 1I).

M1 polarization was achieved by supplementing macrophage GM with 20 ng/mL interferon-gamma (IFN-γ, R&D Systems, Minneapolis, MN, USA) and 100 ng/mL lipopolysaccharide (LPS, Sigma-Aldrich, Taufkirchen, Germany), whereas M2 polarization was induced using 20 ng/mL interleukin 4 (IL-4) and 20 ng/mL interleukin 13 (IL-13) (both from R&D Systems, Minneapolis, MN, USA). Cells assigned to the M0 control and experimental groups were cultured in macrophage GM without polarizing agents for the same duration [42]. During the 72-h polarization period, cells were exposed to one of the following treatments: negative control, 1 µM DEXA, PLA, 0.1% DEXA–PLA, or 1% DEXA–PLA. As it was made with MSCs, printed TS were placed in contact with the culture medium using 6.5-mm Transwell® membrane inserts for 24-well plates (Figure 1H). Based on the DEXA doses reported by others [43], 1 µM DEXA as a pharmacological positive control was selected to ensure a clearly detectable shift in macrophage inflammatory readouts. The aim was not to mimic physiological concentrations

but to validate assay responsiveness and define an upper benchmark for comparison with material-mediated delivery.

On experimental day 5, cell culture supernatants were collected, cleared by centrifugation (300× g, 5 min), and stored at −80 ◦C for the subsequent cytokine analysis. Adherent cells were washed twice with 1 mL of Ca^{2+}/Mg^{2+}-free PBS to remove residual non-adherent cells. Cell metabolic activity and gene expression analyses were subsequently performed on the adherent cell population.

2.11. Cell metabolic activity

Cell metabolic activity was assessed using the resazurin-based AlamarBlue assay (Bio-Rad, Hercules, CA, USA), which measures the reduction of resazurin to resorufin by metabolically active cells. At the indicated time points, culture medium was aspirated and cells were washed twice with 1 mL of sterile Ca^{2+}/Mg^{2+}-free PBS. Fresh macrophage GM containing AlamarBlue reagent (10% v/v) was then added to each well. Wells containing macrophage GM and AlamarBlue reagent (10% v/v) without cells served as blanks. Cells were incubated with the reagent for 4 h at 37 °C in a humidified atmosphere with 5% CO_2. Absorbance of the conditioned medium was measured at 570 nm and 600 nm using a multimode plate reader (Infinite 200 Pro, Tecan, Grödig, Austria). Resazurin reduction was calculated as previously described according to the manufacturer's protocol [42]. Data are reported as relative metabolic activity normalized to the respective control groups.

2.12. RNA extraction and RT-qPCR gene expression analysis

After removal of the culture medium, cell layers were washed twice with 1 mL of sterile Ca^{2+}/Mg^{2+}-free PBS. Total RNA was extracted by adding 350 µL of RLT lysis buffer (Qiagen, Hilden, Germany) directly to the adherent cells, scratching them, and transferring the entire volume to a microcentrifuge tube. The sample was then stored at −80 °C until purification using the RNeasy Mini Kit (Qiagen, Hilden, Germany), following the manufacturer's instructions. RNA concentration and purity (A260/A280 ratio) were determined using a NanoQuant plate in a spectrophotometer (Infinite 200 Pro, Tecan, Grödig, Austria). Complementary DNA (cDNA) was synthesized from DNase-treated RNA (1 µg input) using the iScript cDNA Synthesis Kit (Bio-Rad, Hercules, CA, USA) in a 20 µL reaction volume according to the manufacturer's protocol. RT-qPCR was performed using iTaq Universal SYBR Green Supermix (Bio-Rad, Hercules, CA, USA) with a cDNA input corresponding to 8 ng of RNA per reaction in a total volume of 10 µL. Amplification was carried out on a CFX96 Touch Real-Time PCR Detection System (Bio-Rad, Hercules, CA, USA) using commercially available human gene-specific

primers (Qiagen, Hilden, Germany). The cycling conditions were: 95°C for 30 s, followed by 40 cycles of 95°C for 5 s and 60°C for 30 s. Melting curve analysis was conducted to confirm amplification specificity. All reactions were run in triplicate. Gene expression levels were normalized by geometric averaging of multiple internal control genes (*GAPDH*, *HPRT1*, and *RPL13A*) according to [44], and relative expression was calculated using the $2^{-\Delta\Delta Ct}$ method, with the corresponding negative control group (untreated MSCs at day 7 or M0 macrophages) used as the calibrator [45].

2.13. Cytokine quantification in cell-conditioned medium

Prior to measurement, samples were thawed on ice. Cytokine concentrations were quantified using a human inflammatory Cytometric Bead Array (CBA) kit (BD Biosciences, San Diego, CA, USA) according to the manufacturer's instructions. The assay simultaneously measured the levels of IL-8, IL-1β, IL-6, IL-10, TNF, and IL-12p70. Data acquisition was performed on a FACSCalibur flow cytometer (BD Biosciences, San Jose, CA, USA). Cytokine concentrations were calculated from standard curves generated for each analyte using FCAP Array software (BD Biosciences, Franklin Lakes, NJ, USA). The lower limits of detection were 3.6 pg/mL (IL-8), 7.2 pg/mL (IL-1β), 2.5 pg/mL (IL-6), 3.3 pg/mL (IL-10), 3.7 pg/mL (TNF), and 1.9 pg/mL (IL-12p70).

2.14. Statistical analysis

Statistical analyses were performed using GraphPad Prism (version 10.4.1 for Windows, GraphPad Software, Boston, MA USA). Water contact angle and DEXA release profile were analyzed using ordinary one-way or two-way ANOVA (treatment × time), respectively, followed by Tukey's multiple comparisons test. Cell-based assays were analyzed using the Kruskal–Wallis test followed by Dunn's multiple comparisons test. Four independent experiments were performed (n = 4), each with two technical replicates. Data are presented as mean ± SEM or as box-and-whisker plots (median, interquartile range, minimum–maximum). Statistical significance was defined as $p < 0.05$.

3. Results

3.1. Filament appearance and surface integrity are preserved after DEXA incorporation

Digital microscopic analysis confirmed that DEXA incorporation does not induce detectable changes in filament appearance (color, transparency), surface integrity (no visible aggregates

or defects), or morphological uniformity within the resolution limits of digital microscopy at 100× magnification (Figure 1F).

3.2. Thermal and thermomechanical properties of composite filaments are largely preserved after DEXA incorporation

Table 2 summarizes the parameters extracted from the thermal and thermomechanical characterization of PLA and DEXA-loaded PLA filaments.

Thermal degradation occurred in a single step with onset temperatures between 339.6 and 343.7 °C. The relative residual mass of all samples ranges from 0.4% (PLA) to 0.9% (1% DEXA–PLA) (Figure 2A).

The DSC curves of the second heating run show only minor differences in the qualitative behavior between the PLA and DEXA–PLA (0.1% or 1%) samples. T_g, determined from the inflection point of the heat-flow step, was approximately 61 °C for all samples. All samples exhibited an exothermic cold-crystallization peak at approximately 124 °C followed by a melting peak at approximately 154 °C (Figure 2B). A slight decrease in H_c and a corresponding increase in H_m were observed with increasing DEXA content. Furthermore, no crystallization was observed during the cooling run (data not shown).

Consistent with the DSC results, DMA measurements revealed only minor differences between formulations. Prior to softening, all filaments exhibited storage moduli of approximately 2000 MPa, while the softening temperature ranged from 63.1 °C (0.1% DEXA–PLA) to 64.7 °C (PLA) (Figure 2C).

The glass transition temperature determined from the tan(δ) peak maximum ranged from 74.0 °C for PLA to 76.1 °C for 1% DEXA–PLA (Figure 2D).

Table 2. Summary of the parameters extracted from the thermal and thermomechanical characterization.

Parameter	PLA	0.1% DEXA–PLA	1% DEXA–PLA
T_{onset} (TGA) [°C]	343.7 ± 3.0	339.6 ± 4.9	339.6 ± 0.1
$m_{residual}$ [%]	0.4 ± 0.2	0.6 ± 0.0	0.9 ± 0.0
T_g (DSC) [°C]	61.1 ± 0.1	61.0 ± 0.5	61.1 ± 0.1
T_c (DSC) [°C]	124.1 ± 0.1	124.4 ± 0.5	123.4 ± 0.1
T_m (DSC) [°C]	154.4 ± 0.1	154.6 ± 0.8	154.8 ± 0.3
H_c (DSC) [J/g]	-18.2 ± 1.0	-22.3 ± 1.6	-25.2 ± 2.6
H_m (DSC) [J/g]	17.6 ± 0.1	22.0 ± 0.8	24.6 ± 1.2
T_{onset} E' (DMA) [°C]	64.7 ± 1.9	63.1 ± 0.0	64.1 ± 0.1

T_g (DMA) [°C]	74.0 ± 3.2	75.7 ± 1.0	76.1 ±0.7

PLA, polylactic acid; DEXA, dexamethasone. **Analytical methods:** TGA, thermogravimetric analysis; DSC, differential scanning calorimetry; DMA, dynamic mechanical analysis. **Thermal parameters:** T_{onset}, onset temperature; T_g, glass transition temperature; T_c, crystallization temperature; T_m, melting temperature. **Thermodynamic parameters:** H_c, crystallization enthalpy; H_m, melting enthalpy.

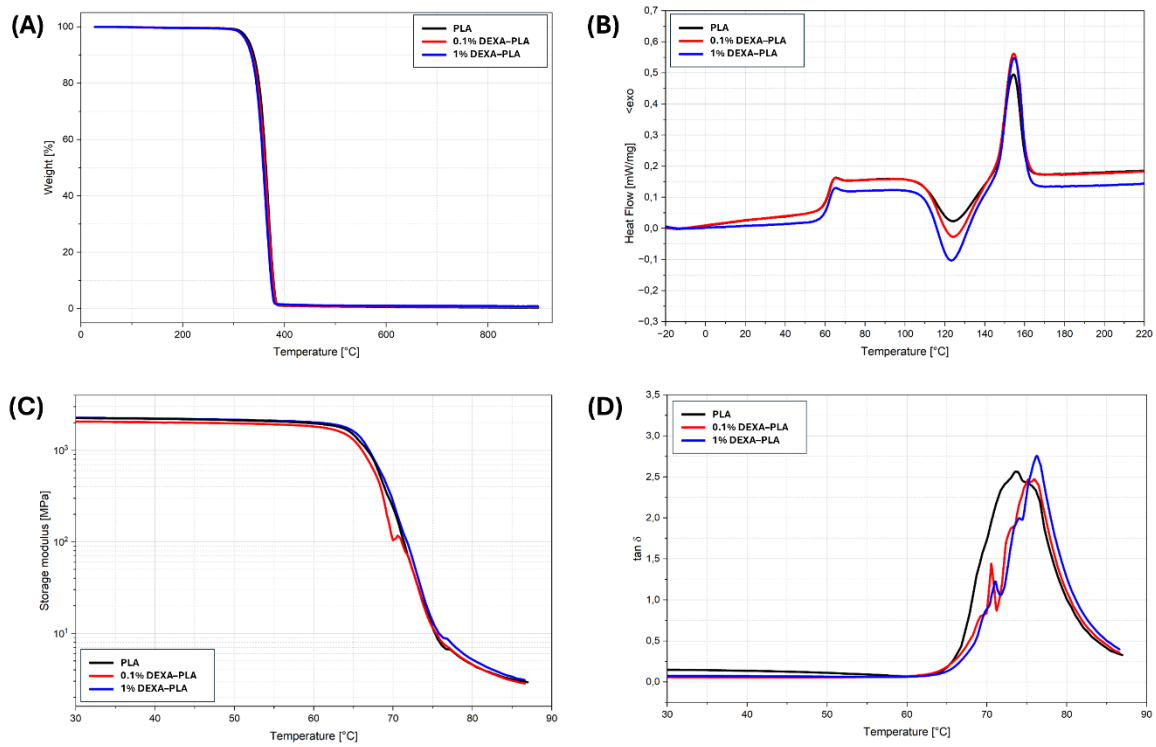

Figure 2. Thermal and thermomechanical properties of PLA and DEXA-loaded PLA filaments. (A) Thermogravimetric analysis (TGA). (B) Differential scanning calorimetry (DSC). (C) Dynamic mechanical analysis (DMA). (D) Glass transition temperature (T_g) determined from the tan(δ) peak maximum.

3.3. DEXA incorporation and thermal aging do not induce detectable chemical modifications in composite filaments

All unaged samples exhibited the characteristic absorption bands of PLA, including the carbonyl stretching vibration at approximately 1750 cm^{-1} and the C–O stretching bands in the 1200–1000 cm^{-1} region. No additional absorption bands were detected following dexamethasone phosphate disodium incorporation (Figure 3A, Table S1).

Difference spectra obtained by subtracting the PLA reference spectrum revealed subtle concentration-dependent intensity changes. The DEXA-containing formulations exhibited

subtle differences in band intensities relative to PLA. Increased signal intensity in the CH_2/CH_3 regions was most pronounced in the 1% DEXA–PLA formulation, whereas differences within the carbonyl and C–O regions were more evident in the 0.1% DEXA–PLA formulation. However, no substantial peak shifts were observed (Figure 3B).

Following thermal aging at 150 °C for 48 h, all samples retained the characteristic PLA absorption pattern. No new absorption bands or shoulder formations were detected, particularly in the carbonyl region around 1750 cm^{-1}. In addition, peak positions remained largely unchanged after aging (Figure 3C).

Difference spectra of the aged samples revealed changes in relative band intensities, most notably within the C–O stretching region. However, no additional absorption bands or peak shifts were detected after thermal treatment (Figure 3D).

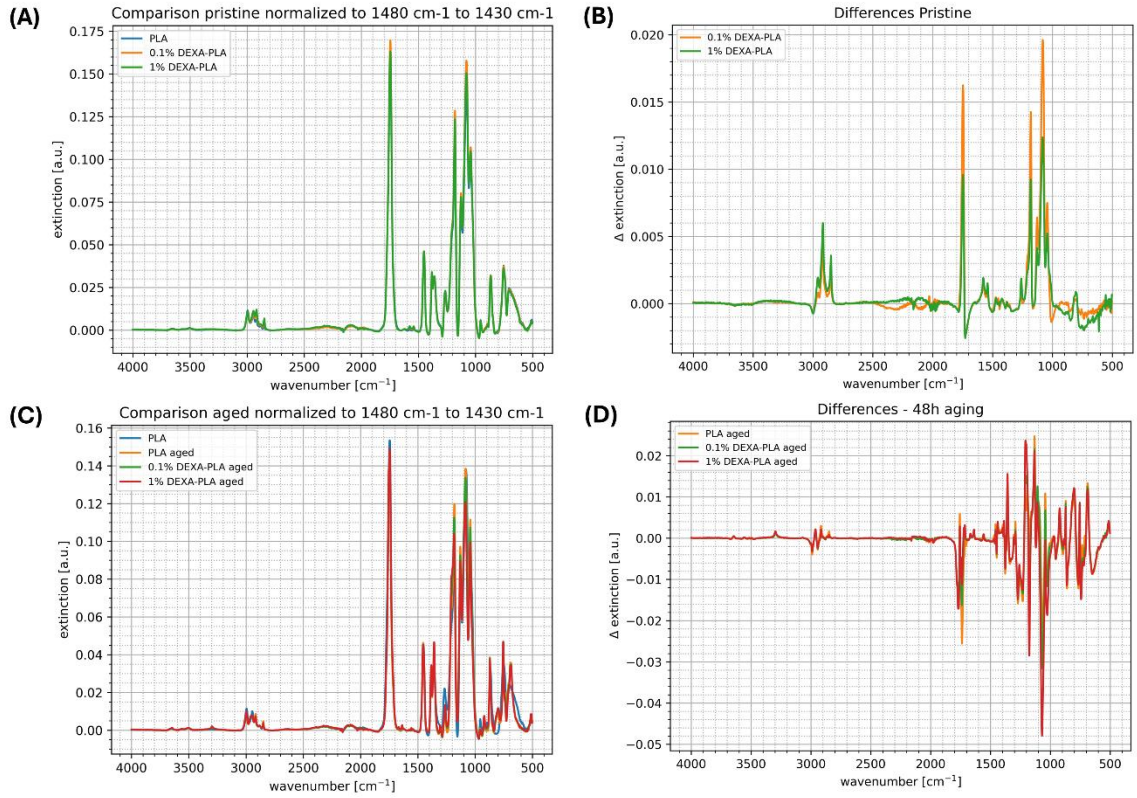

Figure 3. Fourier-transform infrared spectroscopy (FTIR) analysis of PLA and DEXA-loaded PLA filaments before and after thermal aging. (A) ATR-FTIR spectra of unaged PLA, 0.1% DEXA–PLA, and 1% DEXA–PLA showing characteristic PLA absorption bands, including the carbonyl stretching band (~1750 cm^{-1}) and C–O stretching region (1200–1000 cm^{-1}). (B) Difference spectra of unaged samples obtained by subtraction of the PLA reference spectrum, highlighting concentration-dependent intensity variations. (C) ATR-FTIR spectra of samples after thermal aging at 150 °C for 48 h, showing preservation of the characteristic PLA

fingerprint. (D) Difference spectra of aged samples relative to PLA, indicating minor changes in relative band intensities without the appearance of new absorption bands or peak shifts.

3.4. DEXA-loaded PLA specimens showed unchanged surface hydrophobicity

WCA measurements showed that adding DEXA did not significantly affect surface hydrophobicity among groups ($p > 0.05$). Mean ± SEM WCA values (°) were: PLA = 114.4 ± 3.2; 0.1% DEXA–PLA = 111.9 ± 5.0; and 1% DEXA–PLA = 112.8 ± 4.7.

3.5. DEXA incorporation did not affect bending performance

Three-point bending analysis showed no significant differences in flexural modulus or maximum load between PLA and DEXA-loaded PLA composite filaments (Figure 4).

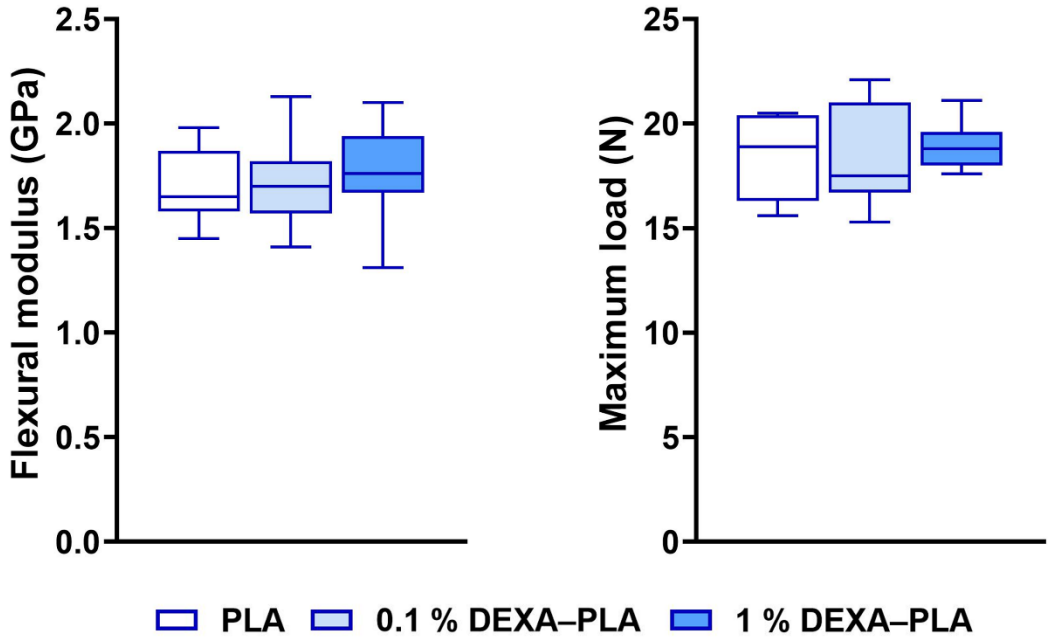

Figure 4. Mechanical performance of rectangular specimens (50 mm × 6 mm × 1 mm) fabricated from PLA or DEXA-loaded PLA filaments. Three-point bending tests were performed with midpoint loading at 2 mm/min until failure. Load and displacement were recorded continuously, and flexural modulus and maximum load were determined from the resulting load–displacement curves.

3.6. DEXA release profile varies strongly with composite DEXA content

The two DEXA loadings generated clearly distinct concentration profiles over the assessed period (Figure 5). After 1 h of incubation, approximately 20.44 ng and 144.15 ng of DEXA per g of test specimen were detected in the incubation medium for the 0.1% and 1% DEXA–PLA

groups, respectively. This represents 0.0044% and 0.0013% of the total DEXA loadings (0.025 mg and 0.25 mg, respectively, assuming a specimen mass of ~25 mg).

In the 0.1% DEXA–PLA group, the measured DEXA concentration increased progressively from 1 h to 72 h, reaching a maximum at 72 h, followed by a decline and stabilization at lower levels at later time points (168–672 h). In contrast, the 1% DEXA–PLA specimens exhibited approximately constant DEXA concentrations in the incubation medium (~143 ng/g of scaffold) across all time points (1–672 h).

Statistical analysis confirmed a significant main effect of time ($p < 0.0001$), formulation ($p < 0.0001$), and time × formulation interaction ($p < 0.0001$).

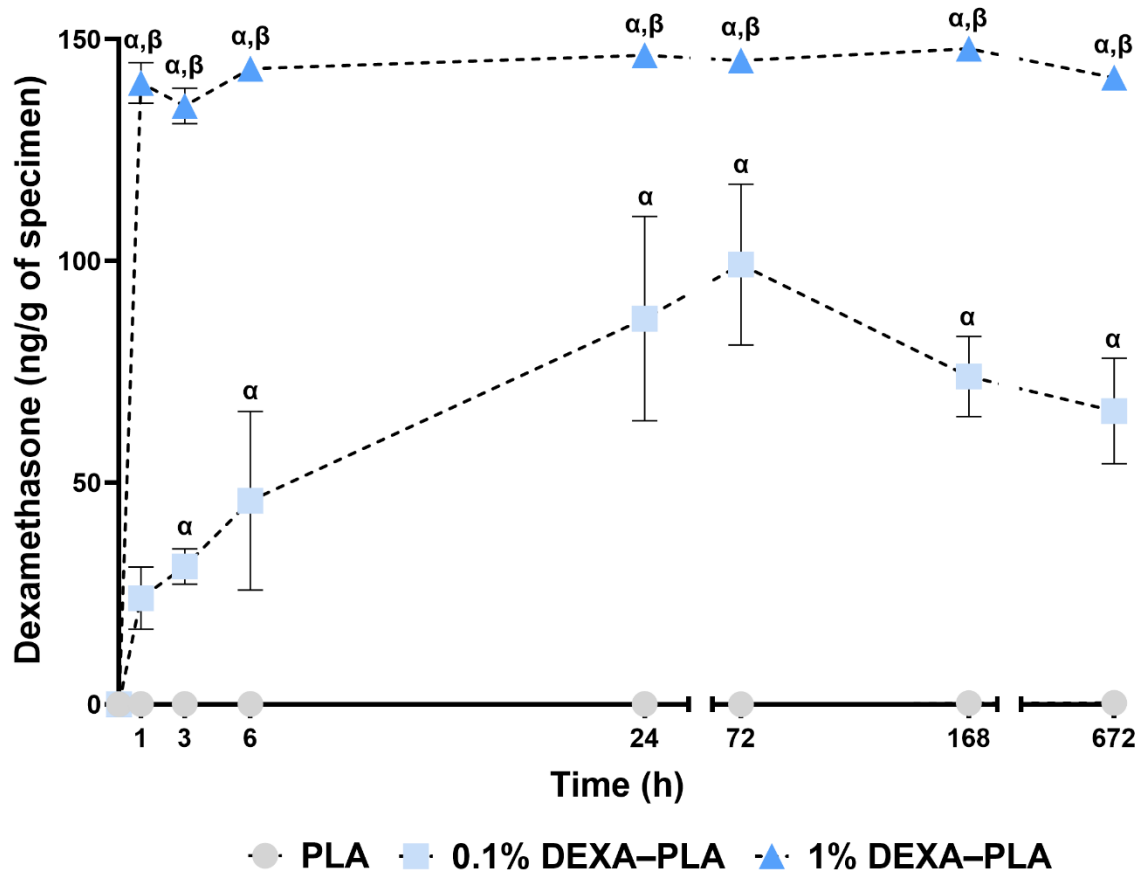

Figure 5. In vitro DEXA concentration in PBS following exposure to DEXA-loaded PLA test specimens (TS). Disc-shaped TS fabricated from PLA (drug-free), 0.1% DEXA–PLA, or 1% DEXA–PLA composite filaments were incubated individually in 100 µL of Ca^{2+}/Mg^{2+}-free PBS at 37°C and 5% CO_2. At the indicated time points, the incubation medium was collected and stored at −80°C until analysis. DEXA concentrations were quantified using an ELISA assay. α: $p < 0.05$ vs. PLA; β: $p < 0.05$ vs. 0.1 % DEXA–PLA.

3.7. MSC metabolic activity is not affected by DEXA-loaded PLA composite filaments

The assessment of MSC metabolic activity showed that neither soluble nor composite-released DEXA affected this parameter after 7 days of OD treatment ($p > 0.05$), while after 14 days, a significant reduction in metabolic activity was observed in the groups supplemented with soluble DEXA at 10 nM compared with the DEXA-free ODM ($p = 0.0014$). In contrast, no significant changes were detected in any of the groups exposed to DEXA–PLA composite filaments compared to their PLA control at the latest time point (Figure 6A).

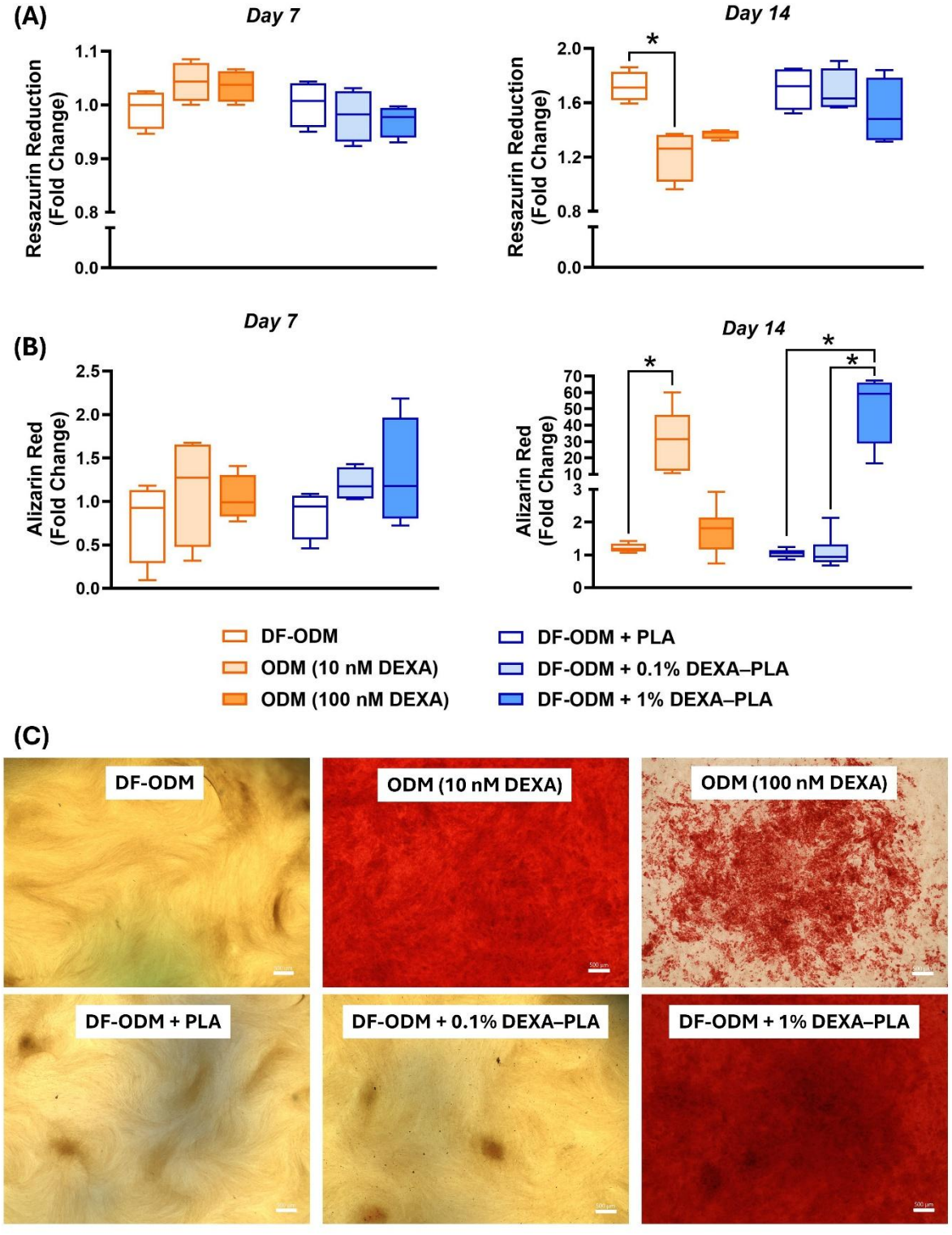

Figure 6. Effect of soluble and composite-released DEXA on MSC metabolic activity and ECM mineralization. (A) Metabolic activity assessed by resazurin (AlamarBlue) reduction after 7 and 14 days of culture. (B) Quantification of Alizarin Red (AR) S staining after 7 and 14 days of culture. (C) Representative phase-contrast images of MSC cultures stained with AR after 14 days of treatment. Scale bar = 500 µm. Experimental groups included DEXA-free (DF)

osteogenic differentiation medium (ODM), ODM supplemented with soluble DEXA (10 or 100 nM), DF-ODM with PLA control test specimen, and DF-ODM with DEXA–PLA composite test specimens (0.1% or 1%). MSCs cultured in growth medium for 7 or 14 days served as reference and were set to 1. *$p < 0.05$.

3.8. MSC osteogenic differentiation is supported by 1% DEXA–PLA composite filament

Spectrophotometric quantification of AR staining revealed no significant changes in ECM calcium deposits produced by soluble or composite-released DEXA at day 7 of OD treatment. Conversely, a significant increase in ECM mineralization was observed after 14 days in cells treated with ODM supplemented with 10 nM soluble DEXA compared with the ones exposed to DEXA-free ODM ($p < 0.0001$). In addition, MSCs exposed to the 1% DEXA–PLA composite filament exhibited significantly higher AR staining compared with the PLA control group ($p = 0.0009$) (Figure 6B and C).

3.9. MSC osteogenic gene expression is altered by 1% DEXA–PLA composite filament

Gene expression analysis revealed distinct, concentration- and delivery-dependent effects of DEXA on osteogenic marker expression over time. After 7 days of OD, MSCs exposed to the 1% DEXA–PLA composite filament showed a transcriptional pattern similar to that induced by 10 nM soluble DEXA, characterized by downregulation of the early osteogenic marker *RUNX2* and upregulation of *ALPL*. At this time point, the 1% DEXA–PLA induced a similar upregulation of *DKK1* as 100 nM soluble DEXA. Additionally, 10 nM soluble DEXA downregulated *COL1A1* and *SPP1* expression (Figure 7A).

After 14 days of OD, gene expression differences were more selective. Cells cultured in ODM supplemented with 10 nM soluble DEXA exhibited significant downregulation of *COL1A1*, while exposure to 100 nM soluble DEXA led to significant upregulation of *SPP1*. In addition, an upregulation of ALPL was observed in the group exposed to the 1% DEXA–PLA composite filament at this later time point (Figure 7B).

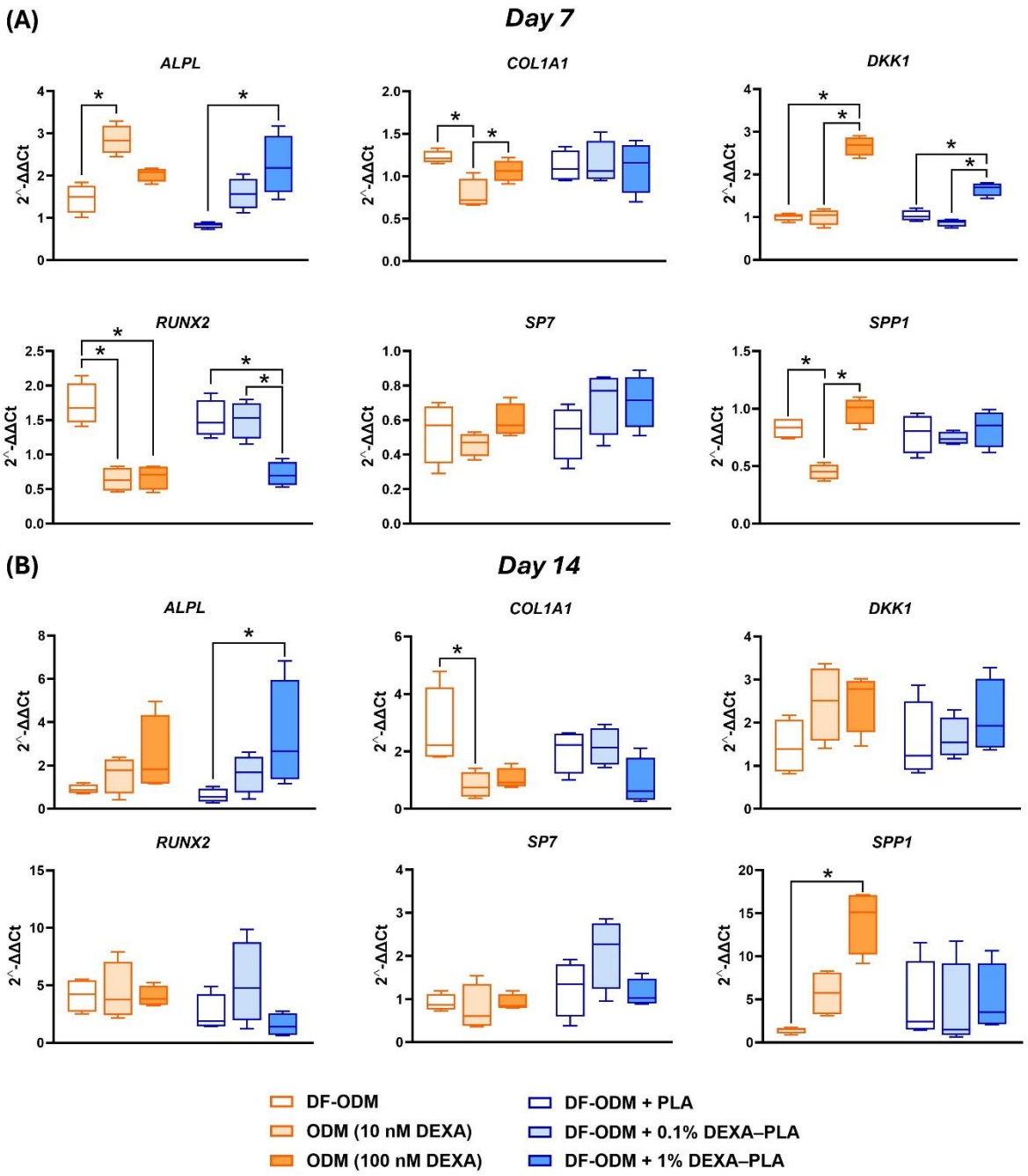

Figure 7. Effect of soluble and composite-released DEXA on osteogenic marker expression by MSCs after 7 (A) and 14 days (B) of treatment. Experimental groups included DEXA-free (DF) osteogenic differentiation medium (ODM), ODM supplemented with soluble DEXA (10 or 100 nM), DF-ODM with PLA control test specimen, and DF-ODM with DEXA–PLA composite test specimens (0.1% or 1%). MSCs cultured in growth medium for 7 or 14 days served as reference and were set to 1. *$p < 0.05$.

3.10. Metabolic activity of M1 THP-1–derived macrophages is reduced by 1% DEXA–PLA composite filament

Exposure to 1 µM soluble DEXA significantly reduced MA, assessed by resazurin reduction, in M0, M1, and M2 TDM compared with their respective untreated controls. Similarly, treatment with the 1% DEXA–PLA composite filament significantly decreased metabolic activity in M1-polarized macrophages compared with its respective PLA control ($p < 0.0001$), whereas no significant effects were observed in M0 or M2 phenotypes. In addition, treatment with the 0.1% DEXA–PLA composite filament did not significantly affect metabolic activity in any macrophage phenotype compared with their respective PLA controls (Figure 8).

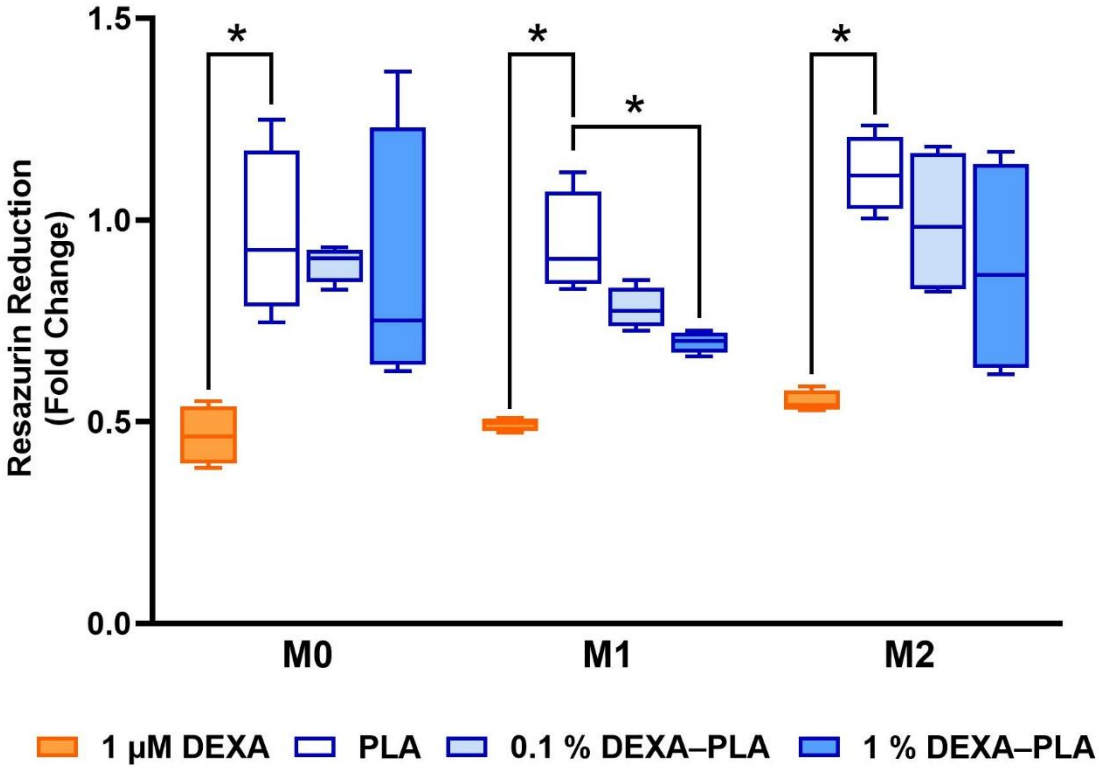

Figure 8. Effect of soluble and composite-released DEXA on metabolic activity of M0, M1, and M2 TDM. Metabolic activity was assessed by resazurin reduction in adherent cells following exposure to soluble DEXA (1 µM), PLA or DEXA–PLA (0.1% or 1%) test specimens during the polarization period. M0 cells cultured in growth medium served as reference and were set to 1. *$p < 0.05$.

3.11. Downregulation of M1- and upregulation of M2-associated markers in TDM by 1% DEXA–PLA composite filament

Gene expression analysis of M1-associated markers in M0, M1, and M2 TDM showed that exposure to 1 µM soluble DEXA resulted in significant downregulation of *CD86* expression in

both M0 and M1 TDM, and *IL1B* expression in M1 TDM compared with their respective PLA control. A significant reduction in *IL1B* expression was also observed in M1 macrophages exposed to the 1% DEXA–PLA composite. No significant changes were detected in other M1-associated genes under the conditions tested (Figure 9A).

The analysis of M2-associated marker genes in THP-1–derived M0, M1, and M2 macrophages showed that both soluble DEXA (1 μM) and the 1% DEXA–PLA composite significantly increased *CD163* expression across all macrophage phenotypes and *PPARG* only in the M1 phenotype compared with the respective PLA control. In addition, exposure to the 1% DEXA–PLA composite resulted in a significant upregulation of *IL10* expression in M2 macrophages (Figure 9B).

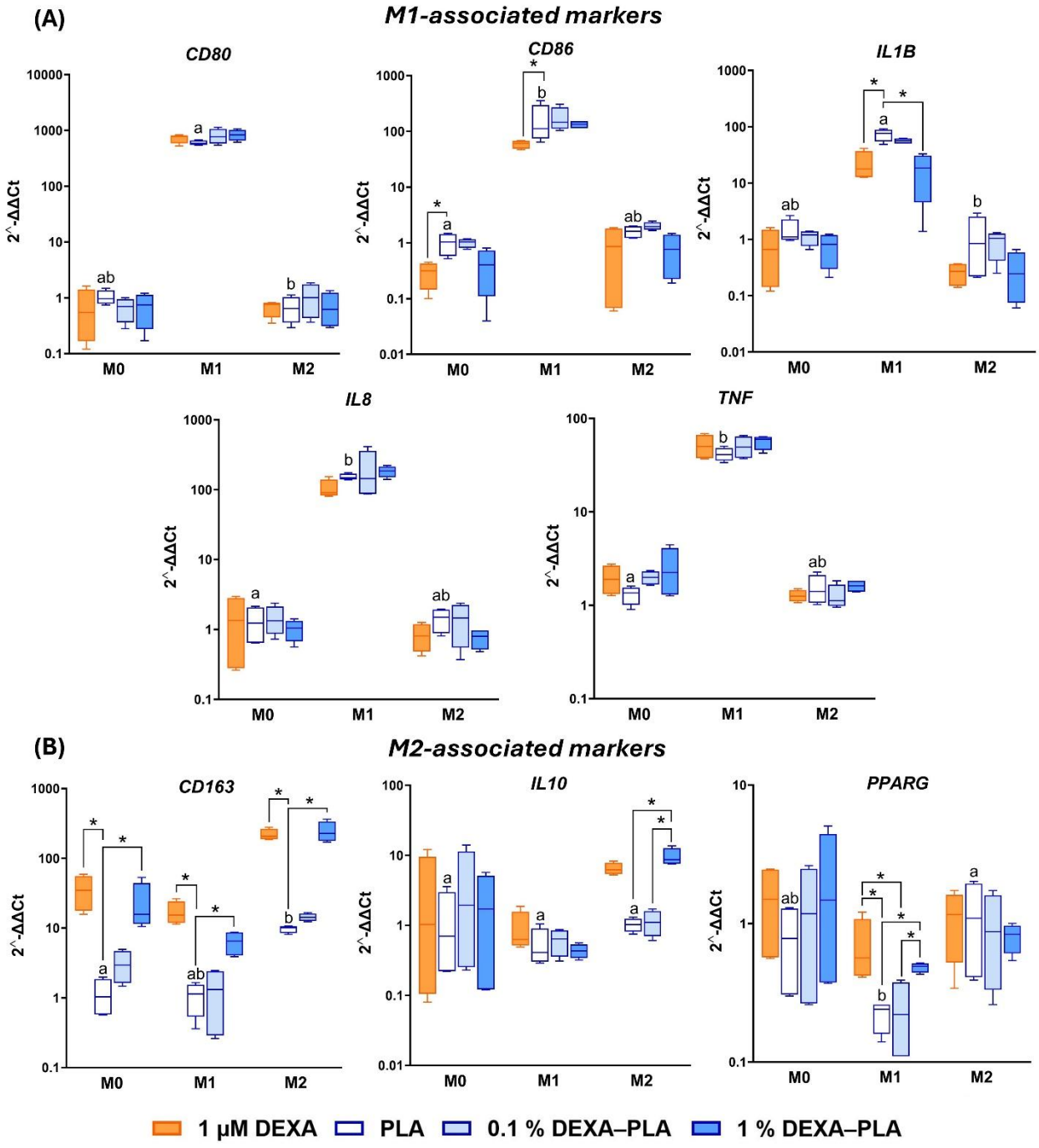

Figure 9. Effect of soluble and composite-released DEXA on the expression of M1- and M2-associated markers (A and B, respectively) in TDM. Gene expression was analyzed by RT-qPCR in adherent cells following exposure during the polarization period to soluble DEXA (1 µM), PLA control specimens, or DEXA–PLA composite test specimens (0.1% or 1%). Statistical differences between PLA groups are denoted by lowercase letters; groups not sharing the same letter are significantly different. M0 cells cultured in growth medium served as reference and were set to 1. *$p < 0.05$.

3.12. Reduction of pro-inflammatory cytokines in M1 TDM by 1% DEXA–PLA composite filament

Comparison of cytokine levels in culture supernatants of adherent M1 TDM following exposure to soluble or composite-released DEXA during polarization showed that 1 μM soluble DEXA and the 1% DEXA–PLA significantly reduced the secretion of IL-1β, IL-6 and TNF-α compared with the respective control group. In addition, IL-6 and TNF levels were significantly lower in these groups compared with the 0.1% DEXA–PLA. The cytokine profile assessed in adherent M0 and M2 cells showed no significant changes produced by any of the treatments (Figure 10).

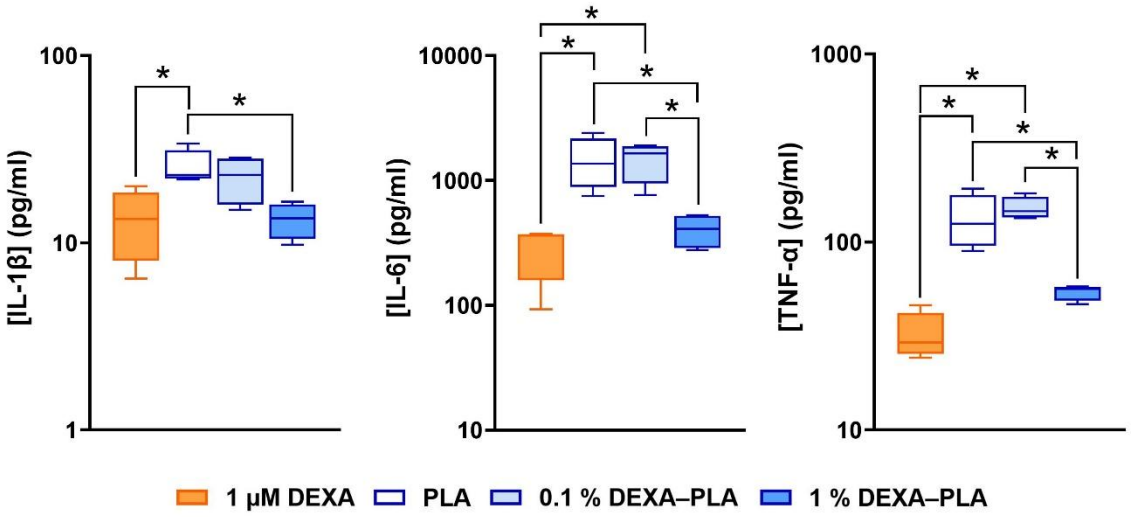

Figure 10. Cytokine secretion by M1 TDM following soluble or composite-mediated DEXA exposure. Cytokine levels in culture supernatants were quantified in adherent cells following exposure during the polarization period to soluble DEXA (1 μM), PLA control specimens, or DEXA–PLA composite test specimens (0.1% or 1%). *$p < 0.05$.

4. Discussion

The fabrication of DEXA-loaded PLA composite filaments in this study was intentionally designed to combine material simplicity, process robustness, and translational relevance.

The present study demonstrates that an FFF-compatible DEXA–PLA composite filament containing 1% DEXA (w/w) provides sustained local DEXA release within a biologically active concentration range and exerts functional effects comparable to soluble DEXA in vitro, indicating that composite-mediated delivery preserves the pharmacological activity of the drug. This formulation promoted osteogenic differentiation of MSCs, as evidenced by sustained

ALPL gene expression and enhanced ECM mineralization, without compromising cell metabolic activity. Furthermore, the composite selectively modulated macrophage polarization by attenuating pro-inflammatory M1-associated gene markers and cytokine secretion while supporting transcriptional programs associated with alternative activation.

Together, our findings confirm the biological efficacy of the DEXA–PLA system and support its potential as a dual-function osteoinductive and immunomodulatory scaffold material for BTE applications.

Compared with previously reported dexamethasone-containing filaments and additively manufactured constructs [8,25-27], the present system offers several practical advantages, including the use of the highly water-soluble and thermal stable phosphate salt form of DEXA, a single-step solvent-free melt-compounding process, and the production of standard 1.75 mm FFF-compatible filaments. The physicochemical characterization further demonstrated that these manufacturing benefits were achieved without compromising the filament appearance and surface integrity, and thermal stability, viscoelastic properties, or chemical integrity of the PLA matrix. Together, these characteristics support manufacturing simplicity, broad printer compatibility, and translational scalability while preserving the biological functionality of the incorporated drug.

4.1. Physicochemical integrity of the DEXA–PLA system

The absence of surface defects and visible aggregates in digital microscopic analysis suggests uniform drug distribution. Poor dispersion or aggregation of fillers within polymer composites has been associated with heterogeneous material properties and may adversely affect the mechanical performance and printability of FFF filaments [46]. In line with this observation, both surface integrity and mechanical performance were largely preserved after DEXA incorporation within the investigated concentration range.

Another critical aspect for drug-loaded filaments processed via FFF is the thermal stability of the active ingredient. The use of dexamethasone phosphate disodium, which exhibits a melting point of 233–240 °C [31], represents a key advantage of the present formulation because it exceeds the temperatures used during filament extrusion (175–189 °C) and 3D printing (185°C). Although melting point or decomposition temperature does not directly indicate the temperature at which biological activity is lost, our experimental findings provide strong evidence that the drug's pharmacological integrity is preserved.

TGA showed a single-step degradation profile for all formulations, with onset temperatures consistent with literature values for PLA filaments [47]. The slight decrease in onset temperature

in DEXA-containing samples may reflect the lower thermal stability of the drug but remains negligible at the investigated concentrations. The marginally increased residual mass in 1% DEXA–PLA may be linked to incomplete decomposition of phosphate-containing species under inert atmosphere [48].

The DSC parameters were consistent with values reported for PLA filaments [49]. Thermal transitions were largely preserved upon DEXA incorporation. Glass transition, melting behavior, and crystallization–melting enthalpies remained comparable across formulations. The increase in H_c and H_m with higher DEXA content may indicate a weak nucleating effect, as reported for other low-molecular-weight additives [50]. Previous analyses have shown that dexamethasone phosphate disodium influences crystallization and thermomechanical properties [31]. Nevertheless, no crystallization was observed during cooling, suggesting that crystallization was kinetically limited under the applied processing conditions. Furthermore, the enthalpies of crystallization and fusion of the respective samples are approximately equal, so that an amorphous material can be assumed for the intended application.

DMA confirmed similar storage moduli across all samples prior to softening. While the softening temperature closely matched the DSC-derived T_g without systematic dependence on DEXA content, the tan(δ)-derived T_g showed a slight shift toward higher temperatures in DEXA-containing samples. This may indicate mildly restricted chain mobility, although bulk viscoelastic properties remain largely unaffected [51].

FTIR spectroscopy confirmed that no covalent interactions or chemical modifications occur between PLA and dexamethasone phosphate disodium. All characteristic PLA bands were preserved, and no new peaks or shifts were detected after drug incorporation or aging. Subtle concentration-dependent intensity changes in CH_2/CH_3, C=O, and C–O regions likely arise from band overlap and changes in polymer packing or crystallinity rather than chemical interactions. FTIR analyses indicate filament stability, with no new absorption bands appearing and the carbonyl region showing no shoulders or additional peaks. This behavior is consistent with previous reports [52,53].

Thermal aging at 150 °C for 48 h did not induce detectable degradation. FTIR spectra of aged samples retained the PLA fingerprint without new bands or carbonyl shoulder formation. Minor intensity variations, particularly in the C–O region, are consistent with crystallinity or morphological changes rather than oxidation [52,53]. Since aging was performed below the melting temperature, structural rearrangements could occur without matrix breakdown.

Collectively, these results demonstrate that dexamethasone phosphate disodium is physically incorporated within a structurally stable PLA matrix without detectable chemical modification

of either component. The preservation of thermal transitions, viscoelastic behavior, and characteristic FTIR bands after drug incorporation and thermal aging is consistent with the physical entrapment strategy described by Maia et al., in which drug release is governed primarily by diffusion and matrix relaxation rather than covalent bond cleavage [54].

4.2. Influence of DEXA loading on release profile

The analysis of in vitro DEXA release over time revealed formulation-dependent kinetics. Both composites released only a small fraction of their total drug content; however, stable DEXA concentrations were detected over 28 days, corresponding to theoretical concentrations relevant for osteogenic and immunomodulatory effects. The 0.1% formulation exhibited an initial increase followed by a decline, whereas the 1% formulation rapidly reached a sustained plateau. Similar sustained release behavior has been reported for DEXA-containing PCL-based systems [8,55]. These findings indicate that the degree of DEXA loading not only affects the absolute amount of released drug but also fundamentally alters release kinetics, which may critically shape downstream cellular responses.

4.3. Composite-mediated DEXA delivery preserves MSC metabolic activity

In the present study, assessment of resazurin reduction indicated that neither DEXA–PLA composite formulation affected cellular metabolic activity, while soluble DEXA significantly reduced it after prolonged exposure. Importantly, resazurin reduction reflects cellular redox and overall metabolic activity rather than cell viability [56]. Accordingly, the observed reduction in metabolic activity following prolonged exposure to soluble DEXA may reflect GC-induced metabolic reprogramming rather than cytotoxicity. This interpretation is supported by previous reports showing that DEXA can alter mitochondrial function and cellular redox homeostasis in MSCs [57], and that exposure to DEXA released from scaffolds containing 0.05–0.25% DEXA did not negatively affect MSC viability [55]. Notably, composite-mediated delivery from the 1% formulation maintained metabolic activity and osteogenic responsiveness, suggesting a more controlled cellular exposure profile.

4.4. Osteogenic responses of MSCs induced by DEXA–PLA composite

The synthetic GC DEXA has been widely included as a critical supplement in OD protocols, together with organic phosphate and ascorbic acid, as it appears essential for full maturation of MSCs into mineral-producing osteoblasts (reviewed in [58]). In line with previous reports, our results show that DEXA-free ODM failed to induce calcium deposition, whereas supplementation with 10 nM DEXA or exposure to the 1% DEXA–PLA composite filament

significantly promoted ECM mineralization [59]. In contrast, the highest dose of soluble DEXA (100 nM) induced only limited ECM mineralization. Together, these observations indicate the existence of an optimal concentration window, close to physiological levels, required to achieve efficient osteoblastic differentiation and ECM mineralization. This dose-dependent response is consistent with GC-mediated regulation of osteogenic signaling pathways, where excessive exposure may impair mineralization [57].

GCs such as DEXA exert dose- and time-dependent effects on MSC biology, influencing proliferation, viability, and OD programs. Indeed, analysis of the pooled data revealed that the effects of DEXA on the proliferation and differentiation of human MSCs are, to a degree, dissociable [19]. In vitro, exposure to high DEXA concentrations at 1000 nM has been reported to inhibit cell proliferation and promote adipogenic commitment, whereas lower concentrations (0.1-100 nM) can support MSC proliferation and OD [17,57,60,61].

Gene expression analysis further revealed concentration- and delivery-dependent effects of DEXA with temporal specificity. At day 7, both soluble DEXA and the 1% DEXA–PLA suppressed *RUNX2* and upregulated *DKK1*, consistent with GC-mediated modulation of osteogenic commitment and canonical Wnt signaling (reviewed in [62]). Similar interactions between glucocorticoids, RUNX2, and Wnt signaling have been reported previously [63]. RUNX2 inhibition is a widely recognized mechanism underlying GC-mediated effects on bone formation [64,65]. However, *RUNX2* mRNA levels do not necessarily reflect functional activity, since GC regulation of RUNX2 is known to involve post-transcriptional and post-translational mechanisms (reviewed in [66,67]).

Despite this shared early transcriptional signature with soluble DEXA, ECM mineralization at day 14 was significantly higher in the 1% DEXA–PLA group. This coincided with sustained upregulation of *ALPL*, whereas soluble 10 nM DEXA induced *ALPL* only transiently at day 7. Given the established role of alkaline phosphatase in hydroxyapatite deposition and matrix mineralization [68,69], sustained ALPL expression may represent a key determinant of effective mineral formation in the composite-treated group.

Although GCs have been reported to suppress type I collagen synthesis [70-73], the sustained reduction of *COL1A1* expression observed at 10 nM DEXA did not translate into complete impaired mineralization but could explain why AR was lower than in the 1% DEXA–PLA group. This could also reflect the temporal sequence of OD, in which collagen matrix deposition precedes and supports subsequent mineralization.

After 14 days of treatment, soluble DEXA exerted dose-dependent transcriptional effects. Treatment with 10 nM DEXA further suppressed *COL1A1*, consistent with glucocorticoid-

mediated inhibition of early matrix gene expression [74,75], whereas 100 nM DEXA significantly upregulated *SPP1*, a marker associated with matrix remodeling and late osteogenic differentiation (reviewed in [75,76]). This biphasic response highlights the context- and dose-dependent regulatory role of DEXA, whereby lower concentrations predominantly suppress collagen synthesis, while higher concentrations favor remodeling-associated pathways.

4.5. Selective effects of DEXA–PLA composites on macrophage metabolic activity

GCs are steroid hormones with key physiological roles in stress responses, metabolism, and immune regulation, particularly through their potent anti-inflammatory effects [77]. In line with this, exposure to 1 μM soluble DEXA uniformly reduced metabolic activity across M0, M1, and M2 TDM. This broad suppression is consistent with previous reports showing that DEXA impairs macrophage glycolysis and overall metabolic function via downregulation of key glycolytic regulators, such as PFKFB3, in both monocyte-derived and tissue-resident macrophages [78,79]. At supraphysiological concentrations, GCs therefore appear to override phenotype-specific metabolic programs.

In contrast, exposure to the 1% DEXA–PLA selectively reduced metabolic activity in M1-polarized macrophages, while sparing M0 and M2 phenotypes. This phenotype-specific effect suggests that this composite delivers a moderate dose modulating macrophage metabolism in a more controlled manner compared with soluble dosing. M1 macrophages are characterized by high glycolytic flux and strong dependence on pro-inflammatory signaling pathways, while M2 macrophages rely predominantly on fatty acid oxidation and oxidative phosphorylation, maintaining an intact tricarboxylic acid cycle (reviewed in [80]). These metabolic signatures can explain the differential susceptibility to DEXA effect and may reflect in M1 cells both metabolic reprogramming and early phenotypic shifts toward a less inflammatory state. Nevertheless, because the AlamarBlue assay reflects overall cellular redox status rather than specific metabolic pathways, it was not possible to discriminate whether the observed changes originated from glycolytic or oxidative processes to confirm a metabolic reprogramming [56].

4.6. Suppression of M1-associated inflammation and promotion of pro-regenerative macrophage polarization by DEXA–PLA composites

Beyond direct metabolic effects, GCs are well recognized to promote macrophage repolarization from a pro-inflammatory M1 phenotype toward a more anti-inflammatory, M2-like state at both transcriptional and secretory levels [77]. In the present study, soluble DEXA significantly downregulated the M1-associated markers *CD86* and *IL1B* in M1 macrophages, confirming its canonical anti-inflammatory activity. CD86 is a costimulatory molecule

associated with pro-inflammatory activation, while IL-1β is a central mediator of M1-driven inflammatory signaling (reviewed in [81,82]). Their suppression is therefore consistent with GC-mediated inhibition of NF-κB–dependent transcription [83-85]. Importantly, exposure to the 1% DEXA–PLA reproduced part of this anti-inflammatory signature, reducing *IL1B* expression in M1 macrophages. This indicates that composite DEXA release is sufficient to attenuate key inflammatory gene programs. However, the transcriptional effects were more selective compared with soluble DEXA, further supporting the concept that delivery mode influences the magnitude and specificity of GC responses.

At the level of M2-associated markers, both soluble DEXA and the 1% DEXA–PLA composite significantly increased *CD163* expression across macrophage phenotypes. CD163 is a scavenger receptor associated with anti-inflammatory and tissue-remodeling macrophages, and its upregulation by GCs has been consistently reported in human, rodent, and porcine macrophages [86,87]. In addition, upregulation of *PPARG* in M1 macrophages exposed to the 1% DEXA–PLA further supports the concept of GC-driven phenotypic reprogramming, as PPARγ is a known regulator of alternative macrophage activation and may contribute to the abovementioned CD163 induction. Consistent with our findings, Iraji Asiabadi et al. reported that macrophages cultured on an electrospun DEXA-loaded scaffold exhibited reduced expression of *TNF* and *NFKB* together with increased *CD163* expression [88].

Another transcriptional change produced by the 1% DEXA–PLA was the upregulation of *IL10* expression in M2 TDM, indicating reinforcement of an anti-inflammatory program, since IL-10 is a hallmark cytokine involved in resolution of inflammation and tissue repair [80,89,90]. In contrast, other studies on human macrophages reported a downregulating effect on *IL10* which was attributed to GC-mediated inhibition of NF-κB [88,91,92].

Depending on their polarization state, macrophages secrete pro-inflammatory and tumor-suppressing (M1) or anti-inflammatory and tissue remodeling (M2) factors (reviewed in [93,94]). In the present study, exposure to the 1% DEXA–PLA significantly suppressed IFN-γ/LPS-induced secretion of IL-1β, IL-6 and TNF-α by M1 macrophages, mirroring the transcriptional changes already described and demonstrating functional suppression of inflammatory mediator release. These findings are consistent with previous reports describing suppression of M1-associated cytokines—including IL-1β, IL-6, IL-23, IL-27, GM-CSF, and TNF family members—by soluble DEXA [77], as well as reduced IL-6 secretion in macrophages cultured on DEXA-containing scaffolds [25]. The reduction of IL-6 and TNF-α was significantly stronger in the 1% DEXA–PLA group compared with the 0.1% DEXA–PLA, indicating a dose-dependent immunomodulatory effect at the composite level. Together, these results confirm that

composite-released DEXA effectively modulates inflammatory cytokine secretion in a manner comparable to soluble GC treatment.

4.7. Limitations

While this study demonstrates promising FFF processability and biological efficacy of DEXA–PLA composite filaments, several limitations should be acknowledged.

First, drug distribution homogeneity and long-term composite degradation behavior were not analyzed. Characterization of these parameters would provide important insight into the stability and sustained performance of the system.

Second, DEXA release was evaluated under static in vitro conditions, which do not reflect the dynamic environment of bone defects, where fluid flow, enzymatic activity, and tissue interactions may influence release kinetics.

Third, the biological evaluation was conducted in monoculture systems, which do not capture the complexity of the in vivo bone healing niche or cell–cell interactions. Fourth, although the disc-shaped TS provides a well-defined, reproducible geometry for testing DEXA release and biological activity, their non-porous architecture differs from the interconnected pore structure typically required for cell infiltration, adhesion, and tissue integration in implantable scaffolds. In addition, the performance of the filament in prosthesis manufacturing was not assessed in this study. Although DEXA addition had only a minimal effect on the thermomechanical properties of the material, its influence on implant morphology and on the 3D printing of complex structures should be further evaluated. Finally, osteogenic assessment relied on selected gene expression markers and endpoint mineralization without detailed analysis of matrix composition or mechanical properties. These aspects warrant further investigation in advanced in vitro models and in vivo studies to support clinical validation.

5. Conclusion

Collectively, our findings demonstrate that an FFF-compatible DEXA–PLA composite filament containing 1% DEXA enables controlled local DEXA delivery within an osteoinductive and immunomodulatory concentration range. This formulation promotes sustained *ALPL* expression and enhanced ECM mineralization by MSC while selectively attenuating pro-inflammatory macrophage activation and supporting M2-associated transcriptional programs. Notably, these effects mirror those observed with defined soluble DEXA concentrations, indicating that composite-mediated delivery preserves the drug's pharmacological activity.

Importantly, these biological outcomes were achieved without compromising the physicochemical integrity of the system, since appearance, surface integrity, mechanical performance, thermal stability, viscoelastic properties, or chemical integrity of the PLA matrix were largely preserved after drug incorporation and processing. By integrating scalable fabrication with preserved material performance and dual osteogenic and immunoregulatory functionality, the DEXA–PLA system confirms its biological efficacy and translational potential as a bioactive, additively manufactured bone replacement scaffold material.

Acknowledgments

The authors gratefully acknowledge Inna Schaible for her technical assistance.

Funding

The work described herein was supported in part by the Moessner Foundation (Moessner Stiftung) located in Frankfurt, Germany.

Conflict of interest

The authors declare they have no competing interests.

Author contributions

Conceptualization: Dirk Henrich, Jonas Neijhoft

Formal analysis: Santiago Bianconi, Cem Asci, Fiona Ott, Ferdinand Mehnert, Robert Heidrich, Michael Wendt, Minhong Wang, Lea Usov, Ingo Marzi

Funding acquisition: Jonas Neijhoft, Dirk Henrich, Ingo Marzi

Investigation: Santiago Bianconi, Cem Asci, Fiona Ott, Ferdinand Mehnert, Robert Heidrich, Michael Wendt, Minhong Wang, Lea Usov

Methodology: Santiago Bianconi, Dirk Henrich, Jonas Neijhoft

Project administration: Dirk Henrich, Ingo Marzi

Resources: Santiago Bianconi, Jonas Neijhoft

Supervision: Santiago Bianconi, Jonas Neijhoft, Dirk Henrich, Ingo Marzi

Validation: Santiago Bianconi, Robert Heidrich, Michael Wendt, Jonas Neijhoft, Lea Usov

Writing–original draft: Santiago Bianconi, Robert Heidrich, Michael Wendt

Ethics approval and consent to participate

The study involved the use of human mesenchymal stromal cells (MSCs) derived from residual bone marrow samples obtained from five healthy adult donors. Ethical approval for the use of these samples for research purposes was granted by the Ethics Committee of the Department of Medicine, Goethe University Frankfurt (approval number 329/10). All donors provided written informed consent prior to sample collection, and the study was conducted in accordance with institutional and national ethical guidelines.

Consent for publication

Not applicable.

Availability of data

Data are available from the corresponding author upon reasonable request.

References

[1] Oryan A, Alidadi S, Moshiri A, et al., 2014, Bone regenerative medicine: classic options, novel strategies, and future directions. J Orthop Surg Res, 9(1):18. https://doi.org/10.1186/1749-799X-9-18

[2] Tsang SJ, van Rensburg AJ, van Heerden J, et al., 2024, The management of critical bone defects: outcomes of a systematic approach. Eur J Orthop Surg Traumatol, 34(6):3225-3231. https://doi.org/10.1007/s00590-024-04050-1

[3] O'Brien FJ, 2011, Biomaterials & scaffolds for tissue engineering. Materials Today, 14(3):88-95. https://doi.org/10.1016/S1369-7021(11)70058-X

[4] Martin I, Simmons PJ, Williams DF, 2014, Manufacturing challenges in regenerative medicine. Sci Transl Med, 6(232):232fs16. https://doi.org/10.1126/scitranslmed.3008558

[5] Grivet-Brancot A, Boffito M, Ciardelli G, 2022, Use of polyesters in fused deposition modeling for biomedical applications. Macromol Biosci, 22(10):2200039.https://doi.org/10.1002/mabi.202200039

[6] Neijhoft J, Ijpma² FFA, 2024, Advances of 3D printing technologies in orthopaedic trauma and surgical training: a transformative approach. Eur J Trauma Emerg Surg, 50(1):1-2. https://doi.org/10.1007/s00068-024-02464-4

[7] Bose S, Roy M, Bandyopadhyay A, 2012, Recent advances in bone tissue engineering scaffolds. Trends Biotechnol, 30(10):546-554. https://doi.org/10.1016/j.tibtech.2012.07.005

[8] Costa PF, Puga AM, Díaz-Gomez L, et al., 2015, Additive manufacturing of scaffolds with dexamethasone controlled release for enhanced bone regeneration. Int J Pharm, 496(2):541-50. https://doi.org/10.1016/j.ijpharm.2015.10.055

[9] Almeida CR, Serra T, Oliveira MI, et al., 2014, Impact of 3-D printed PLA- and chitosan-based scaffolds on human monocyte/macrophage responses: unraveling the effect of 3-D structures on inflammation. Acta Biomat, 10(2):613-22. https://doi.org/10.1016/j.actbio.2013.10.035

[10] Serra T, Ortiz-Hernandez M, Engel E, et al., 2014, Relevance of PEG in PLA-based blends for tissue engineering 3D-printed scaffolds. Mater Sci Eng C Mater Biol Appl, 38:55-62. https://doi.org/10.1016/j.msec.2014.01.003

[11] Shaqour B, Samaro A, Verleije B, et al., 2020, Production of Drug Delivery Systems Using Fused Filament Fabrication: A Systematic Review. Pharmaceutics, 12(6):517. https://doi.org/10.3390/pharmaceutics12060517

[12] Lima AC, Puga AM, Mano JF, et al., 2014, Free and copolymerized γ-cyclodextrins regulate the performance of dexamethasone-loaded dextran microspheres for bone regeneration. J Mater Chem B, 2(30):4943-4956. https://doi.org/10.1039/c3tb21665a

[13] Coutinho AE, Chapman KE, 2011, The anti-inflammatory and immunosuppressive effects of glucocorticoids, recent developments and mechanistic insights. Mol Cell Endocrinol, 335(1):2-13. https://doi.org/10.1016/j.mce.2010.04.005

[14] Kósa JP, Kis A, Bácsi K, et al., 2011, The protective role of bone morphogenetic protein-8 in the glucocorticoid-induced apoptosis on bone cells. Bone, 48(5):1052-7. https://doi.org/10.1016/j.bone.2011.01.017

[15] Jaiswal N, Haynesworth SE, Caplan AI, et al., 1997, Osteogenic differentiation of purified, culture-expanded human mesenchymal stem cells in vitro. J Cell Biochem, 64(2):295-312. doi:10.1002/(SICI)1097-4644(199702)64:2<295::AID-JCB12>3.0.CO;2-I

[16] Lane NE, 2001, An update on glucocorticoid-induced osteoporosis. Rheum Dis Clin North Am, 27(1):235-253. https://doi.org/10.1016/S0889-857X(05)70196-4

[17] Walsh S, Jordan GR, Jefferiss C, et al., 2001, High concentrations of dexamethasone suppress the proliferation but not the differentiation or further maturation of human osteoblast precursors in vitro: relevance to glucocorticoid-induced osteoporosis. Rheumatology (Oxford), 40(1):74-83. https://doi.org/10.1093/rheumatology/40.1.74

[18] DeConde AS, Sidell D, Lee M, et al., 2013, Bone morphogenetic protein-2–impregnated biomimetic scaffolds successfully induce bone healing in a marginal mandibular defect. Laryngoscope, 123(5):1149-1155. https://doi.org/10.1002/lary.23782

[19] Zhang ZZ, Zhang HZ, Zhang ZY, 2019, 3D printed poly(ε-caprolactone) scaffolds function with simvastatin-loaded poly(lactic-co-glycolic acid) microspheres to repair load-bearing segmental bone defects. Exp Ther Med, 17(1):79-90. https://doi.org/10.3892/etm.2018.6947

[20] Pérez-Davila S, Potel-Alvarellos C, Carballo R, et al., 2023, Vancomycin-loaded 3D-printed polylactic acid-hydroxyapatite scaffolds for bone tissue engineering. Polymers (Basel), 15(21):4250. https://doi.org/10.3390/polym15214250

[21] Lee J-H, Baik J-M, Yu Y-S, et al., 2020, Development of a heat labile antibiotic eluting 3D printed scaffold for the treatment of osteomyelitis. Sci Rep, 10(1):7554. https://doi.org/10.1038/s41598-020-64573-5

[22] Cichos S, Schätzlein E, Wiesmann-Imilowski N, et al., 2023, A new 3D-printed polylactic acid-bioglass composite for bone tissue engineering induces angiogenesis in vitro and in ovo. Int J Bioprint, 9(5):751. https://doi.org/10.18063/ijb.751

[23] Schätzlein E, Kicker C, Söhling N, et al., 2022, 3D-printed PLA-bioglass scaffolds with controllable calcium release and msc adhesion for bone tissue engineering. Polymers, 14(12):2389. https://doi.org/10.3390/polym14122389.

[24] Söhling N, Al Zoghool S, Schätzlein E, et al., 2022, In vitro evaluation of a 20% bioglass-containing 3D printable PLA composite for bone tissue engineering. Int J Bioprint, 8(4):602. https://doi.org/10.18063/ijb.v8i4.602

[25] Li X, Wang Y, Wang Z, et al., 2018, Composite PLA/PEG/nHA/Dexamethasone scaffold prepared by 3D printing for bone regeneration. Macromol Biosci, 18(6):1800068. https://doi.org/10.1002/mabi.201800068

[26] Farto-Vaamonde X, Auriemma G, Aquino RP, et al., 2019, Post-manufacture loading of filaments and 3D printed PLA scaffolds with prednisolone and dexamethasone for tissue regeneration applications. Eur J Pharm Biopharm, 141:100-110. https://doi.org/10.1016/j.ejpb.2019.05.018

[27] Chen C-H, Dash BS, Ting W-C, et al., 2024, Bone tissue engineering with adipose-derived stem cells in polycaprolactone/graphene oxide/dexamethasone 3D-printed scaffolds. ACS Biomater Sci Eng, 10(10):6425-6440. https://doi.org/10.1021/acsbiomaterials.4c00774

[28] Moyadee C, Chaloeijitkul K, Wadaugsorn K, et al., 2026, Influence of molecular weight on functional performance and migration of pla food-contact films. Polym Eng Sci 66(6):4422-4430. https://doi.org/10.1002/pen.70510

[29] Backes EH, Pires LdN, Costa LC, et al., 2019, Analysis of the degradation during melt processing of PLA/biosilicate® composites. J Comp Sci, 3(2):52. J Compos Sci, 3(2):52. https://doi.org/10.3390/jcs3020052

[30] Neijhoft J, Weslati H, Eras V, et al., 2026, Granulate-to-filament: an extrusion-mixed pla–human bone material system for 3D-printed bone scaffolds. J Funct Biomater, 17(4):187. https://doi.org/10.3390/jfb17040187

[31] dos Santos J, Balbinot GdS, Buchner S, et al., 2023, 3D printed matrix solid forms: Can the drug solubility and dose customisation affect their controlled release behaviour? Int J Pharm X, 5:100153. https://doi.org/10.1016/j.ijpx.2022.100153

[32] International Organization for Standardization. Plastics — Thermogravimetry (TG) of polymers — Part 1: General principles. ISO 11358-1:2022; 2022.

[33] International Organization for Standardization. Plastics — Differential scanning calorimetry (DSC) — Part 1: General principles. ISO 11357-1:2023; 2023.

[34] International Organization for Standardization. Plastics — Determination of dynamic mechanical properties — Part 1: General principles. ISO 6721-1:2019; 2019.

[35] McKinney W. Data Structures for Statistical Computing in Python. In: *Proceedings of the Python in Science Conference*. SciPy; 2010:56-61. doi:10.25080/majora-92bf1922-00a

[36] Harris CR, Millman KJ, van der Walt SJ, et al., 2020, Array programming with NumPy. Nature, 585(7825):357-362. https://doi.org/10.1038/s41586-020-2649-2

[37] Erb D, 2022, pybaselines: A Python library of algorithms for the baseline correction of experimental data. Zenodo. https://doi.org/10.5281/zenodo.7255880

[38] Hunter JD, 2007, Matplotlib: A 2D graphics environment. Comput sci eng, 9(3):90-95. https://doi. org/10.1109/MCSE

[39] International Organization for Standardization. Plastics — Determination of flexural properties. ISO 178:2019; 2019.

[40] Langenbach F, Handschel J, 2013, Effects of dexamethasone, ascorbic acid and β-glycerophosphate on the osteogenic differentiation of stem cells in vitro. Stem Cell Res Ther, 4(5):117. https://doi.org/10.1186/scrt328

[41] Park EK, Jung HS, Yang HI, et al., 2007, Optimized THP-1 differentiation is required for the detection of responses to weak stimuli. Inflamm Res, 56(1):45-50. https://doi.org/10.1007/s00011-007-6115-5

[42] Bianconi S, Leppik L, Oppermann E, et al., 2024, Direct current electrical stimulation shifts THP-1-derived macrophage polarization towards pro-regenerative m2 phenotype. Int J Mol Sci, 25(13):7272. https://doi.org/10.3390/ijms25137272

[43] Knijff EM, Breunis MN, van Geest MC, et al., 2006, A relative resistance of T cells to dexamethasone in bipolar disorder. Bipolar Disord, 8(6):740-50. https://doi.org/10.1111/j.1399-5618.2006.00359.x

[44] Vandesompele J, De Preter K, Pattyn F, et al., 2002, Accurate normalization of real-time quantitative RT-PCR data by geometric averaging of multiple internal control genes. Genome Biol 3(7):research0034. https://doi.org/ 10.1186/gb-2002-3-7-research0034.

[45] Livak KJ, Schmittgen TD, 2001, Analysis of relative gene expression data using real-time quantitative PCR and the 2(-Delta Delta C(T)) Method. Methods, 25(4):402-8. https://doi.org/10.1006/meth.2001.1262

[46] Wickramasinghe S, Do T, Tran P, 2020, FDM-based 3D printing of polymer and associated composite: a review on mechanical properties, defects and treatments. Polymers (Basel), 12(7). https://doi.org/10.3390/polym12071529

[47] Kervran M, Vagner C, Cochez M, et al., 2022, Thermal degradation of polylactic acid (PLA)/polyhydroxybutyrate (PHB) blends: A systematic review. Polym Degrad Stabil, 201:109995. https://doi.org/10.1016/j.polymdegradstab.2022.109995

[48] Svoboda R, Vrbenský R, Honzíček J, et al., 2025, Thermal stability of dexamethasone-evaluation with regard to modern medicinal and pharmaceutical 3d-printing applications. Molecules, 30(21). https://doi.org/10.3390/molecules30214234

[49] Abas M, Habib T, Noor S, et al., 2022, Parametric investigation and optimization to study the effect of process parameters on the dimensional deviation of fused deposition modeling of 3d printed parts. Polymers (Basel), 14(17). https://doi.org/10.3390/polym14173667

[50] Feng Y, Ma P, Xu P, et al., 2018, The crystallization behavior of poly(lactic acid) with different types of nucleating agents. Int J Biol Macromol, 106:955-962. https://doi.org/10.1016/j.ijbiomac.2017.08.095

[51] Cristea M, Ionita D, Iftime MM, 2020, Dynamic mechanical analysis investigations of PLA-based renewable materials: how are they useful? Materials (Basel), 13(22):5302. https://doi.org/10.3390/ma13225302

[52] Leroy A, Ribeiro S, Grossiord C, et al., 2017, FTIR microscopy contribution for comprehension of degradation mechanisms in PLA-based implantable medical devices. J Mater Sci Mater Med, 28(6):87. https://doi.org/10.1007/s10856-017-5894-7

[53] Rasselet D, Ruellan A, Guinault A, et al., 2014, Oxidative degradation of polylactide (PLA) and its effects on physical and mechanical properties. Eur Polym J, 50:109-116. https://doi.org/10.1016/j.eurpolymj.2013.10.011

[54] Maia FR, Bidarra SJ, Granja PL, et al., 2013, Functionalization of biomaterials with small osteoinductive moieties. Acta Biomat, 9(11):8773-89. https://doi.org/10.1016/j.actbio.2013.08.004

[55] Majrashi M, Kotowska A, Scurr D, et al., 2023, Sustained release of dexamethasone from 3d-printed scaffolds modulates macrophage activation and enhances osteogenic differentiation. ACS Appl Mater Interfaces, 15(49):56623-56638. https://doi.org/10.1021/acsami.3c09774

[56] Rampersad SN, 2012, Multiple applications of Alamar Blue as an indicator of metabolic function and cellular health in cell viability bioassays. Sensors (Basel), 12(9):12347-60. https://doi.org/10.3390/s120912347

[57] Ma L, Feng X, Wang K, et al., 2020, Dexamethasone promotes mesenchymal stem cell apoptosis and inhibits osteogenesis by disrupting mitochondrial dynamics. FEBS Open Bio, 10(2):211-220. https://doi.org/10.1002/2211-5463.12771

[58] Freeman FE, Stevens HY, Owens P, et al., 2016, Osteogenic differentiation of mesenchymal stem cells by mimicking the cellular niche of the endochondral template. Tissue Eng Part A, 22(19-20):1176-1190. https://doi.org/10.1089/ten.TEA.2015.0339

[59] Alm JJ, Heino TJ, Hentunen TA, et al., 2012, Transient 100 nM dexamethasone treatment reduces inter- and intraindividual variations in osteoblastic differentiation of bone marrow-derived human mesenchymal stem cells. Tissue Eng Part C Methods, 18(9):658-666. https://doi.org/10.1089/ten.TEC.2011.0675

[60] Hong L, Sultana H, Paulius K, et al., 2009, Steroid regulation of proliferation and osteogenic differentiation of bone marrow stromal cells: a gender difference. J Steroid Biochem Mol Biol, 114(3-5):180-5. https://doi.org/10.1016/j.jsbmb.2009.02.001

[61] Xiao Y, Peperzak V, van Rijn L, et al., 2010, Dexamethasone treatment during the expansion phase maintains stemness of bone marrow mesenchymal stem cells. J Tissue Eng Regen Med, 4(5):374-86. https://doi.org/10.1002/term.250

[62] Baron R, Kneissel M, 2013, WNT signaling in bone homeostasis and disease: from human mutations to treatments. Nat Med, 19(2):179-92. https://doi.org/10.1038/nm.3074

[63] Morimoto E, Li M, Khalid AB, et al., 2017, Glucocorticoids hijack RUNX2 to stimulate WIF1 for suppression of osteoblast growth and differentiation. J Cell Physiol, 232(1):145-53. https://doi.org/10.1002/jcp.25399

[64] de Melo Pereira D, Eischen-Loges M, Birgani ZT, et al., 2020, Proliferation and osteogenic differentiation of hmscs on biomineralized collagen. Front Bioeng Biotechnol, 8:554565. https://doi.org/10.3389/fbioe.2020.554565

[65] Kim BB, Kim M, Park YH, et al., 2017, Short-term application of dexamethasone on stem cells derived from human gingiva reduces the expression of RUNX2 and β-catenin. J Int Med Res, 45(3):993-1006. https://doi.org/10.1177/0300060517701035

[66] Franceschi RT, Xiao G, 2003, Regulation of the osteoblast-specific transcription factor, Runx2: responsiveness to multiple signal transduction pathways. J Cell Biochem, 88(3):446-54. https://doi.org/10.1002/jcb.10369

[67] Koromila T, Baniwal SK, Song YS, et al., 2014, Glucocorticoids antagonize RUNX2 during osteoblast differentiation in cultures of ST2 pluripotent mesenchymal cells. J Cell Biochem, 115(1):27-33. https://doi.org/10.1002/jcb.24646

[68] Golub EE, Boesze-Battaglia K. The role of alkaline phosphatase in mineralization. *Curr Opin Orthop*. 2007;18(5):444-448. doi:10.1097/bco.0b013e3282630851

[69] Millán JL, 2013, The role of phosphatases in the initiation of skeletal mineralization. Calcif Tissue Int, 93(4):299-306. https://doi.org/10.1007/s00223-012-9672-8

[70] Advani S, LaFrancis D, Bogdanovic E, et al., 1997, Dexamethasone suppresses in vivo levels of bone collagen synthesis in neonatal mice. Bone, 20(1):41-46.https://doi.org/10. https://doi.org/1016/S8756-3282(96)00314-6

[71] Iu MF, Kaji H, Sowa H, et al., 2005, Dexamethasone suppresses Smad3 pathway in osteoblastic cells. J Endocrinol, 185(1):131-138. https://doi.org/10.1677/joe.1.05962

[72] Schlesinger PH, Blair HC, Beer Stolz D, et al., 2020, Cellular and extracellular matrix of bone, with principles of synthesis and dependency of mineral deposition on cell membrane transport. Am J Physiol Cell Physiol, 318(1):C111-c124. https://doi.org/10.1152/ajpcell.00120.2019

[73] Umrath F, Pfeifer A, Cen W, et al., 2022, How osteogenic is dexamethasone?-effect of the corticosteroid on the osteogenesis, extracellular matrix, and secretion of osteoclastogenic factors of jaw

periosteum-derived mesenchymal stem/stromal cells. Front Cell Dev Biol, 10:953516. https://doi.org/10.3389/fcell.2022.953516

[74] Warmink K, Lijnzaad P, Schubert SA, et al., 2025, Mechanisms of dexamethasone-induced bone toxicity in developing bone: a single-cell perspective. JBMR Plus, 9(10). https://doi.org/10.1093/jbmrpl/ziaf146

[75] Si J, Wang C, Zhang D, et al., 2020, Osteopontin in bone metabolism and bone diseases. Med Sci Monit, 26:e919159. https://doi.org/10.12659/msm.919159

[76] Icer MA, Gezmen-Karadag M, 2018, The multiple functions and mechanisms of osteopontin. Clin Biochem, 59:17-24. https://doi.org/10.1016/j.clinbiochem.2018.07.003

[77] Shamekh MM, Lindqvist B, Nalvarte I, 2025, Dexamethasone drives macrophage repolarization linked to increased triple-negative breast cancer aggressiveness. Cell Death Dis, 17(1):114. https://doi.org/10.1038/s41419-025-08363-9

[78] Stifel U, Wolfschmitt EM, Vogt J, et al., 2022, Glucocorticoids coordinate macrophage metabolism through the regulation of the tricarboxylic acid cycle. Mol Metab, 57:101424. https://doi.org/10.1016/j.molmet.2021.101424

[79] Thong L, Sandby Thomas O, O ÓG, et al., 2025, Dexamethasone inhibits Mycobacterium tuberculosis-induced glycolysis but preserves antimicrobial function in primary human macrophages. Sci Rep, 15(1):34310. https://doi.org/10.1038/s41598-025-20188-2

[80] Viola A, Munari F, Sánchez-Rodríguez R, et al., 2019, The metabolic signature of macrophage responses. Front Immunol, 10:1462. https://doi.org/10.3389/fimmu.2019.01462

[81] Mosser DM, Edwards JP, 2008, Exploring the full spectrum of macrophage activation. Nat Rev Immunol, 8(12):958-69. https://doi.org/10.1038/nri2448

[82] Martinez FO, Gordon S, 2014, The M1 and M2 paradigm of macrophage activation: time for reassessment. F1000prime Rep, 6:13. https://doi.org/10.12703/p6-13

[83] De Bosscher K, Schmitz ML, Vanden Berghe W, et al., 1997, Glucocorticoid-mediated repression of nuclear factor-kappaB-dependent transcription involves direct interference with transactivation. Proc Natl Acad Sci U S A, 94(25):13504-9. https://doi.org/10.1073/pnas.94.25.13504

[84] De Bosscher K, Vanden Berghe W, Vermeulen L, et al., 2000, Glucocorticoids repress NF-kappaB-driven genes by disturbing the interaction of p65 with the basal transcription machinery, irrespective of coactivator levels in the cell. Proc Natl Acad Sci U S A, 97(8):3919-24. https://doi.org/10.1073/pnas.97.8.3919

[85] Jeon YJ, Han SH, Lee YW, et al., 2000, Dexamethasone inhibits IL-1β gene expression in LPS-stimulated RAW 264.7 cells by blocking NF-κB/Rel and AP-1 activation. Immunopharmacology, 48(2):173-183. https://doi.org/10.1016/S0162-3109(00)00199-5

[86] Schaer DJ, Boretti FS, Schoedon G, et al., 2002, Induction of the CD163-dependent haemoglobin uptake by macrophages as a novel anti-inflammatory action of glucocorticoids. Br J Haematol, 119(1):239-43. https://doi.org/10.1046/j.1365-2141.2002.03790.x

[87] Takenouchi T, Morozumi T, Wada E, et al., 2021, Dexamethasone enhances CD163 expression in porcine IPKM immortalized macrophages. In Vitro Cell Dev Biol Anim, 57(1):10-16. https://doi.org/10.1007/s11626-020-00535-5

[88] Iraji Asiabadi A, Esmaeil N, Zargar Kharazi A, et al., 2024, Harnessing IL-10 induced anti-inflammatory response in maturing macrophages in presence of electrospun dexamethasone-loaded PLLA scaffold. J Biom Mat Res Part B, App Biom, 112(6):e35411. https://doi.org/10.1002/jbm.b.35411

[89] Peranteau WH, Zhang L, Muvarak N, et al., 2008, IL-10 overexpression decreases inflammatory mediators and promotes regenerative healing in an adult model of scar formation. J Invest Dermatol, 128(7):1852-60. https://doi.org/10.1038/sj.jid.5701232

[90] Sziksz E, Pap D, Lippai R, et al., 2015, Fibrosis Related Inflammatory Mediators: Role of the IL-10 Cytokine Family. Mediators Inflamm, 2015:764641. https://doi.org/10.1155/2015/764641

[91] Cao S, Zhang X, Edwards JP, et al., 2006, NF-kappaB1 (p50) homodimers differentially regulate pro- and anti-inflammatory cytokines in macrophages. J Biol Chem, 281(36):26041-50. https://doi.org/10.1074/jbc.M602222200

[92] Saraiva M, O'Garra A, 2010, The regulation of IL-10 production by immune cells. Nat Rev Immunol, 10(3):170-81. https://doi.org/10.1038/nri2711

[93] Boutilier AJ, Elsawa SF, 2021, Macrophage Polarization States in the Tumor Microenvironment. Int J Mol Sci, 22(13). https://doi.org/10.3390/ijms22136995

[94] Li R, Ye JJ, Gan L, et al., 2024, Traumatic inflammatory response: pathophysiological role and clinical value of cytokines. Eur J Trauma Emerg Surg, 50(4):1313-1330. https://doi.org/10.1007/s00068-023-02388-5